Title
Biochemical Alterations in the Extracellular Matrix in a Murine Model of Duchenne Muscular Dystrophy

Author
Chin, Jesse Wei-lun

Publication Date
2017

Peer reviewed|Thesis/dissertation

UNIVERSITY OF CALIFORNIA

Los Angeles

Biochemical Alterations in the Extracellular Matrix in a Murine Model of Duchenne Muscular Dystrophy

A thesis submitted in partial satisfaction
of the requirements for the degree Master of Science
in Physiological Science

by

Jesse Wei-lun Chin

2017

ABSTRACT OF THE THESIS

Biochemical Alterations in the Extracellular Matrix
in a Murine Model of Duchenne Muscular Dystrophy

by

Jesse Wei-lun Chin

Master of Science in Physiological Science
University of California, Los Angeles, 2017
Professor Rachelle Hope Watson, Chair

Duchenne muscular dystrophy (DMD) is characterized by progressive muscle degeneration due to the absence of the protein dystrophin, and the subsequent loss of the dystrophin-glycoprotein complex, resulting in inflammation, degeneration/regeneration, and a decrease in muscular strength and function. Although the extracellular matrix was previously thought only to provide structural support to resident cells, there is a growing body of evidence implicating it in cell signaling pathways that may negatively affect muscle regeneration. Despite the increasingly acknowledged importance of the matrix, there is still very little we know about how matrix composition may change in DMD. Therefore, we utilize mass spectrometry to quantify biochemical changes that occur in the extracellular matrix in a murine model of DMD. Identification of changes in the matrisome between dystrophic and normal muscle will allow for the identification of future therapeutic targets that may inform the development of successful therapies for DMD.

The thesis of Jesse Wei-lun Chin is approved.

Patricia Emory Phelps

James Akira Wohlschlegel

Rachelle Hope Watson, Committee Chair

University of California, Los Angeles

2017

DEDICATION

I would like to dedicate this thesis to my parents, Hungneng Steve Chin and Chienhua Cathy Chuang. Your support and sacrifices over the past twenty-three years have allowed me to pursue my dreams. I would also like to dedicate this thesis to my girlfriend, Kimberly Hwang. Your belief in me and support in even the most stressful of situations have allowed me to accomplish tasks I never thought possible.

TABLE OF CONTENTS

LIST OF FIGURES

ACKNOWLEDGEMENTS

I would like to thank my mentor Dr. Rachelle H. Watson for her guidance and support over the past two years. Her patience and understanding have been a large part of my success in graduate school and I could not have asked for a better mentor. She has inspired in me not only a passion for research, but also for teaching. I would also like to thank my other committee members, Dr. Patricia E. Phelps and Dr. James Wohlschlegel, for their help and influence. Thank you, Patty, for inspiring me to pursue a graduate education and your guidance before I was even a graduate student. Thank you, James, for your continuing guidance and expertise in proteomics that have advanced this project.

I would also like to thank all of the members of the Crosbie-Watson laboratory. I want to specially thank Kristen Stearns-Reider for all the sacrifices she has made helping guide me through my project. All the advice and support you have all given me have helped me finish my thesis and prepared me for medical school. In addition, I would like to thank Dr. Melissa Sondej for her advice and guidance during our preliminary mass spectrometry trials.

The methods section for how mice were obtained for the study (page 5) was prepared by Dr. Kristen Stearns-Reider for an unpublished manuscript. The protocols for C18 tip cleanup (page 8) and mass spectrometry pipelines (page 8-9) were developed by Dr. James Wohlschlegel.

This work was made possible by the following grants: UCLA CTSI #UL1TR000124, NIH NIAMS R01 #AR048179, and NIH P30 #AR057230.

BACKGROUND

Duchenne muscular dystrophy (DMD) is an X-linked recessive genetic disorder that affects 1 in 5,000 boys [1]. Those affected are wheelchair reliant by their early teen years and have a life expectancy of approximately thirty years. DMD is characterized by progressive muscle degeneration due to the loss of the protein dystrophin, a part of the dystrophin-glycoprotein complex (DGC). The DGC serves as an anchor between the cytoskeletal components of the muscle fiber and the surrounding extracellular matrix. The absence of dystrophin results in loss of the DGC, leading to contraction-induced damage of the sarcolemma that initially results in inflammation, followed by continuous cycles of degeneration and regeneration [2]. Over time, regenerative processes are unable to repair the chronic muscle damage, resulting in an accumulation of fat and fibrotic tissue in the muscle [2, 3]. This ultimately results in a loss of muscular strength and function. At late stages, cardiac and respiratory muscle functions are compromised [4].

Although there is currently no cure for DMD, several therapies are currently under investigation. These include gene therapies aimed at introducing a functional dystrophin gene to muscles throughout the body, as well as cell transplantations that attempt to introduce dystrophin positive cells to muscle [5]. However, these current treatments have had limited success and face several challenges. For gene therapy, the largest obstacle is determining how to package and deliver the large dystrophin gene [5]. For cellular therapies, limited myoblast migration and differentiation result only in local effects around the injection sites [5, 6].

The limited success of current therapies necessitates a broader approach to the development of treatments for DMD, including looking at factors extrinsic to the muscle cell [7]. Although the extracellular matrix was previously thought of as merely a passive structure that

only provided structural support to resident cells, there is a growing body of evidence that implicate it in cell signaling pathways. The matrix has a significant role in controlling myoblast proliferation and differentiation [8]. Decorin, a matrix proteoglycan, inhibits myostatin activity which decreases fibrosis and increases muscle fiber regeneration by increasing myocyte proliferation and differentiation [9, 10]. Furthermore, other extracellular matrix factors are known to modulate intracellular signaling pathways, such as the TGF-β pathway that modulates cell proliferation and fibrosis [11]. Matrix components such as matrix metalloproteinase-9, integrin $\alpha_V\beta_6$, plasmin, and thrombospondin-1 have all been shown to activate latent TGF-β [12-17]. Despite the prominent effects the extracellular matrix has on these signaling pathways, we still know very little about the relative abundance of these components in the dystrophic extracellular matrix.

Interestingly, several of the genetic modifiers and markers of DMD were found to be components of the extracellular matrix, such as osteopontin, latent TGF-β binding protein 4, annexin A6, fibronectin, and lumican [18, 19]. In DMD, the increasingly fibrotic composition of the extracellular matrix is a result of chronic inflammation that leads to unregulated deposition of matrix proteins as well as the replacement of contractile muscle fibers with non-contractile tissue [2, 3]. The accumulation of matrix proteins also forms a physical barrier that may hamper accessibility to the resident cells for targeted therapies [3]. When this inflammation or fibrosis is reduced, improvements in the pathology have been observed. Inhibiting fibrinogen-driven inflammation in muscles reduced both the inflammatory process as well as muscle degeneration [20]. The inhibition of collagen synthesis by halofuginone reduced muscle fibrosis and improved dystrophic pathology [21].

This relationship between the matrix and its resident cells represents a dynamical and reciprocal relationship. Resident cells secrete and produce the surrounding extracellular matrix, and in turn, the matrix affects the activity of the resident cells by upregulating or downregulating their activity. These signaling cascades produced by the matrix are especially relevant in DMD. While it was previously assumed that the eventual decrease in muscle regeneration observed in DMD was a result of reduced satellite cell regeneration, it was recently shown that satellite cells from aged dystrophic muscle have the same regenerative ability as wild type satellite cells when transplanted into a wild type mouse [22]. Therefore, it is not just the loss of dystrophin and the DGC, but also the altered biochemical composition of the matrix that plays a major role in the reduced regeneration observed in DMD.

Administering ECM components has already been found to improve DMD pathology. Biglycan is a matrix proteoglycan that controls sarcolemmal integrity by regulating components of the dystrophin-associated protein complex [23]. Like dystrophic mice, biglycan deficient mice have a sarcolemma that is leaky and susceptible to damage. Administering recombinant biglycan to dystrophic mice ameliorated several pathological markers of DMD with a resultant increase in muscle strength and myofiber size, decrease in the number of centrally located nuclei and decrease in the levels of creatine kinase in the blood [24]. Another potential therapeutic ECM target is laminin, an important protein in the basement membrane of the matrix that facilitates binding of the dystroglycan complex to the extracellular matrix [25]. Laminin-111 treatment of *mdx* mice improved the pathology by increasing muscle strength, sarcolemmal integrity, and resistance to fatigue, reduced inflammation, and reduced exercise-induced damage [6, 26]. When coupled to myoblast transplantation, laminin-111 treatment improved myoblast proliferation and migration compared to myoblast transplantation alone [6]. Coupling cellular therapies to targeted

changes in the biochemical composition of the matrix and its associated factors, or the matrisome [27], may then be a new treatment paradigm for DMD.

Despite the increasingly acknowledged importance of the extracellular matrix in the regulation of muscle cell activity, there is still very little we know about the matrix in terms of its composition or how it changes in DMD. While the composition of collagen in the ECM has been well documented, other areas of the matrisome are not as well understood. Understanding these changes in the matrix will provide a greater picture of the signaling pathways that are affected in DMD. Therefore, we utilize mass spectrometry to understand the biochemical changes that occur in the extracellular matrix in a murine model of DMD, with an emphasis on the glycoproteins that serve as signaling molecules in the matrix. Utilizing two separate decellularization techniques, we hope to determine and compare suitable methods to enrich for extracellular matrix proteins so that they can be adequately identified through mass spectrometry. We hypothesize that the absence of dystrophin and the DGC drives biochemical changes in the dystrophic matrix by upregulating or downregulating proteins in the matrisome. Identification of the changes in the matrisome between dystrophic and normal muscle will provide future therapeutic targets that may improve the success of current cellular therapies.

CHAPTER 1: PROTEOMIC ANALYSIS OF THE ECM WITH TRANSVERSE SECTIONS

Introduction

The extracellular matrix (ECM) makes up only a small fraction of skeletal muscle. To perform biochemical analysis of the ECM, it is necessary to remove any cellular material prior to analysis to avoid any differences being masked by the presence of cellular material. This chapter described the development of protocols to: 1) isolate ECM from skeletal muscle and, 2) prepare ECM samples for proteomic analysis using mass spectrometry. Using these protocols, we will investigate changes in the biochemical properties of the ECM in *mdx* mice (murine model of DMD) relative to healthy wild-type controls.

Materials and Methods

Animals

Wild-type (C57BL/6J) and *mdx* male mice were purchased from Jackson Laboratories (Bar Harbor, ME, USA). Mice were maintained in the Terasaki Life Sciences Vivarium following guidelines established by the Institutional Animal Care and Use Committee at the University of California, Los Angeles (approval #2000-029-43) and approval for these studies was granted by the UCLA Animal Welfare Assurance (approval #A3196-01). All mice used in the study were 18-20 weeks old.

Determination of optimal decellularization time

Tissue preparation

Wild type (n=3) and *mdx* mice (n=3) were euthanized by administering an overdose of isofluorane followed by cervical dislocation. The left and right quadriceps of each mouse were dissected and frozen with liquid nitrogen. Our laboratory previously determined that 30 minutes was the optimal exposure time to 1% SDS to successfully decellularize 30µm muscle sections, as determined by the absence of cellular material and nuclear material following H&E and DAPI staining (unpublished). While this method is best for immunofluorescence analysis of matrix components, it is an inefficient preparation method for the large volume of tissue needed for proteomic analysis. In an effort to maintain uniform section thickness for decellularization, we chose to section tissue at the maximal thickness capability of our cryostat (200 µm). The quadriceps muscles were transversely sectioned into 200µm thick sections at -18°C with a Leica CM3050S Research Cryostat and stored at -80°C (Figure 1-1).

Time series decellularization

Decellularization was performed with 1% SDS for ninety minutes. Every ten minutes, the SDS solution was removed and saved, replaced with fresh 1% SDS, and the decellularization was allowed to continue. The SDS supernatant for each time point was spun down and the resultant pellet or gelatinous homogenate was collected and stored for analysis.

Confirmation of decellularization

SDS-PAGE analysis was used to detect the presence of proteins in each time fraction of

the time series decellularization. Twenty microliters from each time point were loaded with 1XLSB (loading sample buffer), containing SDS, sucrose, tris-HCl – pH7.4, β-mercaptoethanol, and bromophenol blue, on to a 6% SDS-PAGE gel. Gels were cast using the Mini-PROTEAN Tetra Handcast System for 1.5mm thick gels by Bio-Rad (Hercules, CA). A 30% acrylamide/bis solution, 19:1 from Bio-Rad (Hercules, CA) was used for the polyacrylamide stacking and separating gels. Bands were visualized by staining with Coomassie Blue for thirty minutes, followed by an overnight incubation in destain buffer (30% methanol, 10% glacial acetic acid). Imaging was performed with an Epson Perfection V19 scanner.

Determination of optimal decellularization time

Gels were stained with Coomassie Blue to detect whether bands were present in each time fraction. The most prominent band typically occurs between 35 and 55kDa and most likely corresponds to actin. The presence of bands was presumed to be predominantly cellular material being removed from the matrix and ending up in the supernatant. The optimal decellularization time was defined as the time when no bands were detected by Coomassie Blue staining.

Mass spectrometry

Tissue preparation

Four to five hundred milligrams of sectioned tissue per wild type and *mdx* sample were decellularized with 1% SDS at 50rpm for using the optimal time period as determined by the time series decellularization analysis. The samples were then rinsed in subsequent washes with

PBS, ddH_2O, and finally PBS to remove any remaining cellular debris. The wet weight of the remaining insoluble pellet was measured before being frozen and stored at -80°C (Figure 1-2).

Enzymatic digestion

The digestion protocol utilizes an on-pellet digestion as previously described [28]. Samples were resolubilized with urea, reduced with dithiothreitol, and alkylated with iodoacetamide. Glycan residues were removed with PNGaseF from New England Biolabs (Ipswich, MA). Digestion was performed with Lys-C from Thermo Fischer Scientific (Waltham, MA) and trypsin from Thermo Fischer Scientific (Waltham, MA). The samples were spun down and the supernatant was collected for C18 tip cleanup.

C18 tip cleanup

Digested peptides were desalted and concentrated using Pierce C18 tips from Thermo Fisher Scientific (Waltham, MA). The C18 tips were wetted with 50% acetonitrile and equilibrated with 0.1% trifluoroacetic acid before being loaded with sample. The tips were then washed with 0.1% trifluoroacetic acid/ 5% acetonitrile and the peptides were eluted with 60% acetonitrile. The samples were speed vacuumed to near complete dryness and stored at -80°C.

Mass spectrometry

Samples were submitted to the UCLA Proteome Research Center (PRC) for analysis. All analysis was performed utilizing their established data analysis pipeline. In short, peptides were fractionated online with a 75µm inner diameter fritted fused silica capillary column with a [3-4µm] pulled electrospray tip packed in-house with 17cm of Luna C18(2) 3µm reversed phase

particles (Phenomonex) [29, 30]. An acetonitrile gradient was delivered through the column with the Dionex UltiMate™ 3000 ultra high pressure nanoflow liquid chromatography system (Thermo Fischer Scientific) to separate peptides via ultra-high pressure liquid chromatography. MS/MS spectra were produced with an Orbitrap Fusion Lumos (Thermo Fischer Scientific). Fragmentation spectra were searched against theoretical fragmentation spectra generated from a protein database consisting of all mouse ORFs using MS-GF+. The peptide identifications were then filtered at the peptide ($q < 0.01$) and protein level ($q < 0.01$) using decoy database-derived false discovery rates and the Percolator and Fido algorithms, respectively. Peptide-level quantitation was performed by generating MS1-level extracted ion chromatograms using the Skyline software suite and then assessing chromatogram quality using mProphet ($q < 0.01$). Peptide-level quantitation was further analyzed using the MSStats tool to model protein abundances and perform statistical comparisons between wild type and m*dx* samples.

Protein name, gene name, uniport ID, p-value and fold change for all proteins with a significant change of at least $\log_2 1$ between *mdx* vs. wild type were compiled into a table. Extracellular matrix proteins were determined through lists published by the Matrisome Project [31] and compiled into a separate table. Matrix proteins were organized into the groups: collagens, glycoproteins, proteoglycans, ECM regulators, and ECM affiliated proteins.

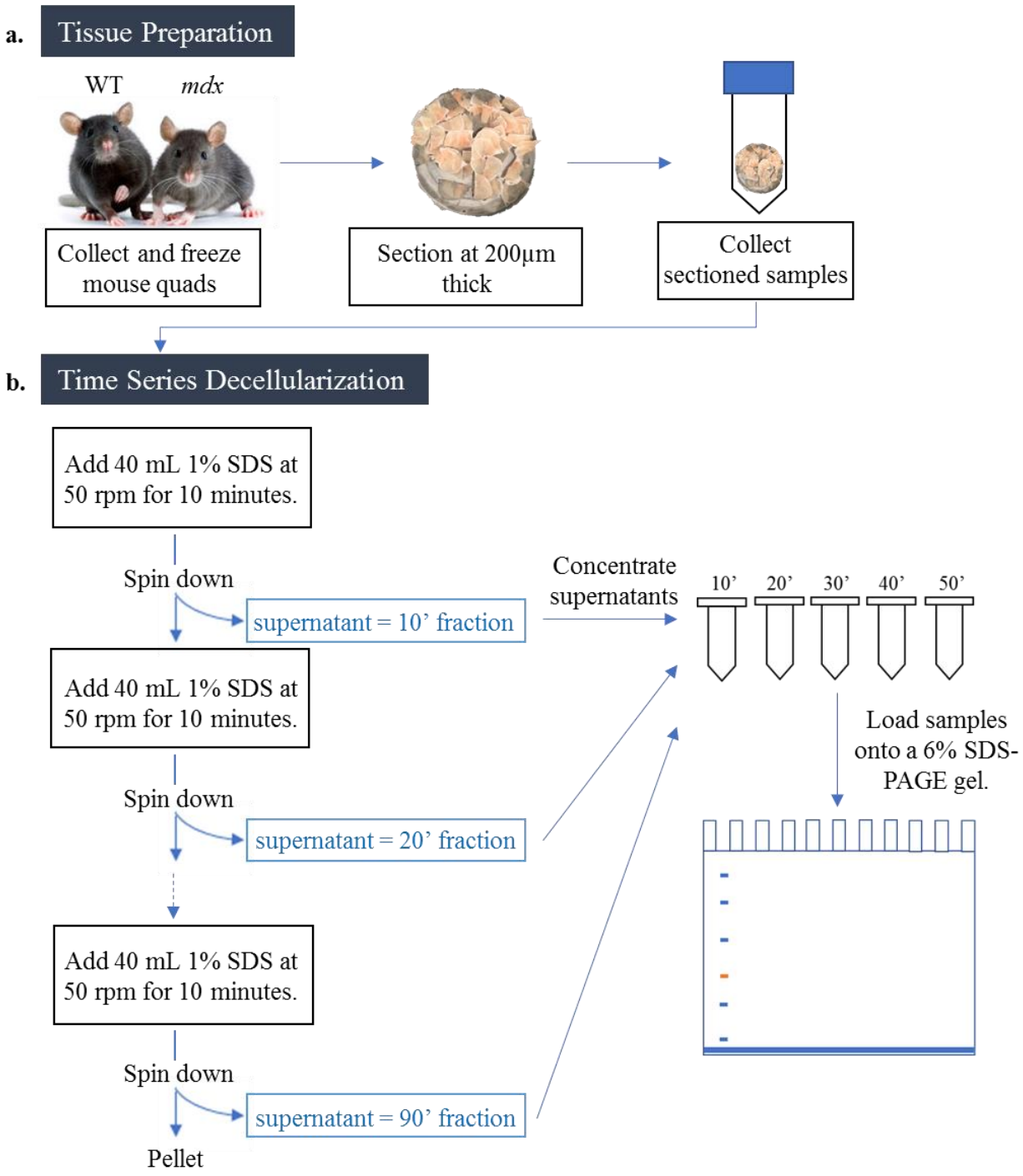

Figure 1-1: Schematic diagram of time series decellularization. (a) Quadriceps were isolated from wild type and *mdx* mice. Tissues were transversely sectioned (200µm) and placed in their respective 50mL conical tubes. (b) Samples were decellularized with 1% SDS. Every ten minutes, the tube was spun down at 3000rpm, supernatant was removed, and placed back on rotator with fresh SDS. Fractions were later concentrated and run on a 6% SDS-PAGE gel to detect whether predicted muscle proteins were present in each time fraction.

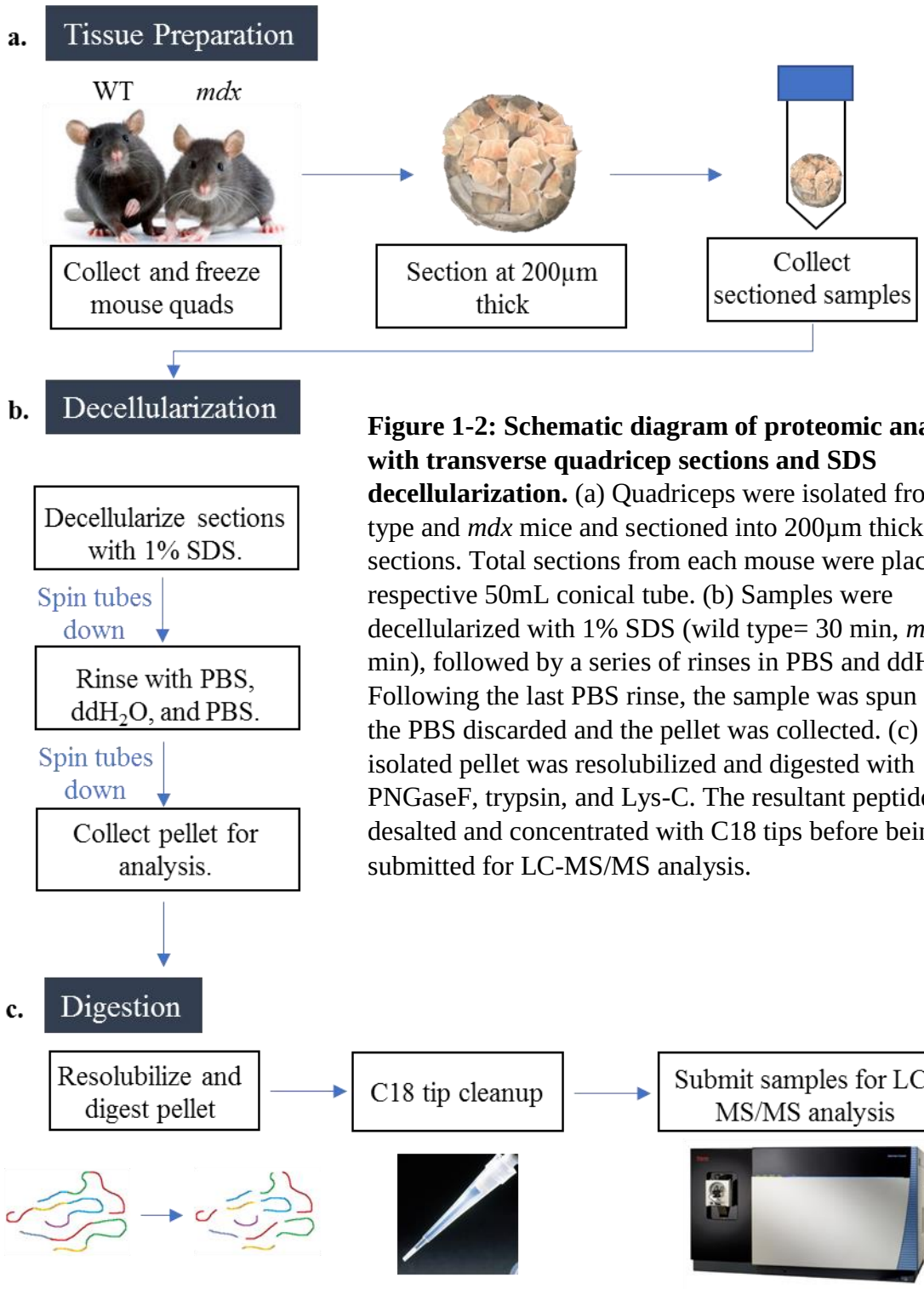

Figure 1-2: Schematic diagram of proteomic analysis with transverse quadricep sections and SDS decellularization. (a) Quadriceps were isolated from wild type and *mdx* mice and sectioned into 200µm thick sections. Total sections from each mouse were placed in a respective 50mL conical tube. (b) Samples were decellularized with 1% SDS (wild type= 30 min, *mdx*= 70 min), followed by a series of rinses in PBS and ddH_2O. Following the last PBS rinse, the sample was spun down, the PBS discarded and the pellet was collected. (c) The isolated pellet was resolubilized and digested with PNGaseF, trypsin, and Lys-C. The resultant peptides were desalted and concentrated with C18 tips before being submitted for LC-MS/MS analysis.

Results

Wild type and mdx sections decellularize at different rates

To determine the optimal time to decellularize wild type and *mdx* samples, we utilized a time series decellularization. Ten-minute supernatant fractions revealed different rates of decellularization between wild type and *mdx* (Figure 1-3). Wild type SDS rinses revealed intense bands in the ten and twenty minute fractions, with feint staining of bands in thirty and forty-minute time fractions. These are presumably cellular proteins as matrix proteins are often resistant to SDS degradation, insoluble, and therefore unable to run through the gel. A noticeable band occurring between 35 and 55kDa is most likely actin and its gradual decrease in intensity suggests the removal of these cellular contaminants. No further bands were detected after forty minutes. *Mdx* sections displayed strongly stained bands in the ten, twenty, and thirty-minute time fractions. Diffuse staining was found in the forty-, fifty-, and sixty-minute fractions. No further bands were detected in time fractions after sixty minutes. These time series decellularizations help validate the time needed to remove the maximum amount of cellular material while still maintaining the matrix proteins. Previous findings by our lab have noted the susceptibility of the wild type matrix to degradation by prolonged SDS treatment. On the contrary, the *mdx* matrix appears to be more resilient and requires more prolonged SDS treatment for adequate removal of cellular material. Based on our findings, and to ensure equal removal of cellular material, we selected thirty minutes as the optimal decellularization time for wild type, and seventy minutes for *mdx* samples.

a. WT

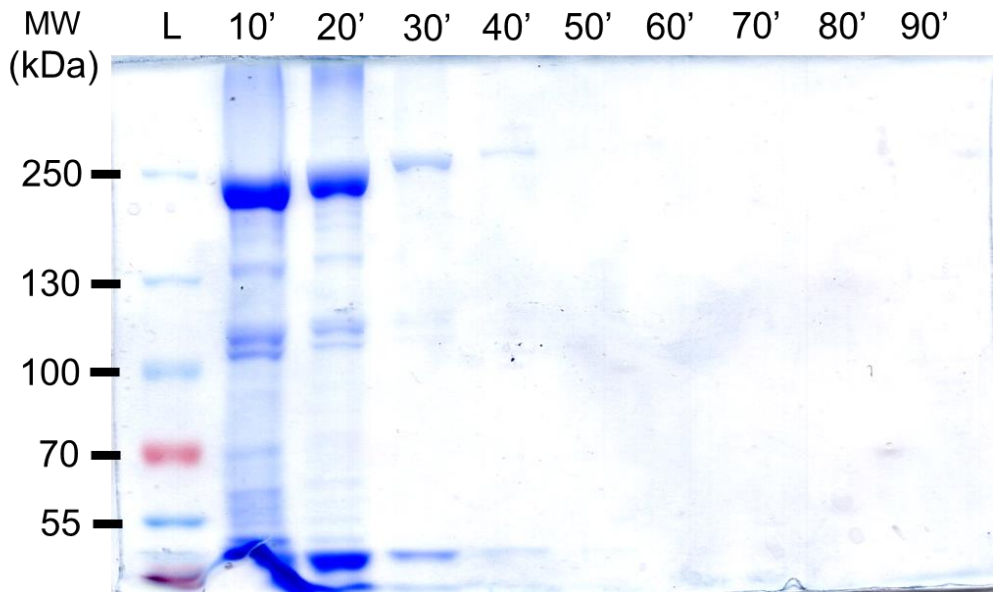

b. *mdx*

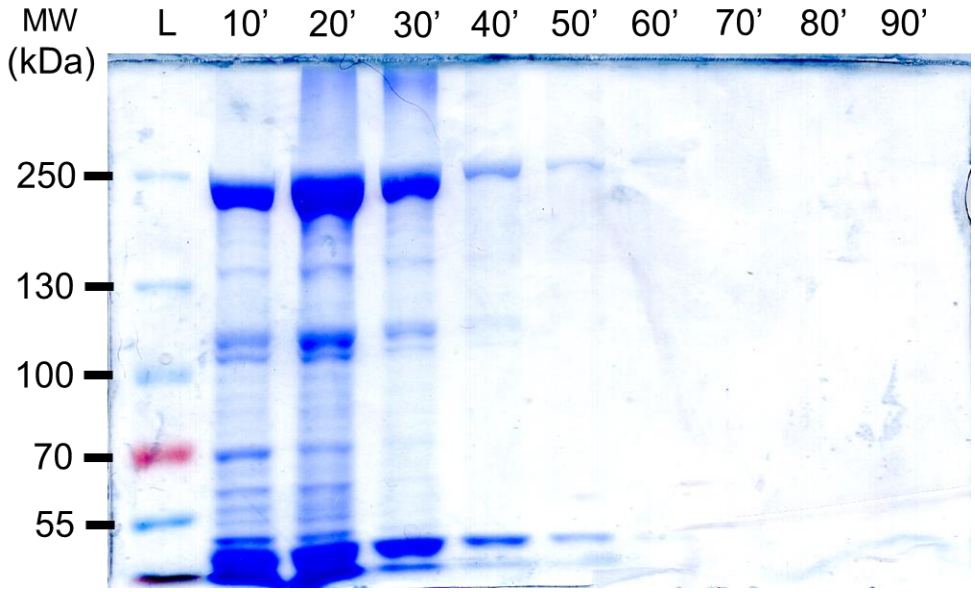

Figure 1-3: Wild type and *mdx* quadricep sections decellularize at different rates. Wild type (a) and *mdx* (b) transverse quadricep sections (200μm) were decellularized with fresh 1% SDS every ten minutes for two hours. The first nine of the ten minute fractions were concentrated and analyzed through SDS-PAGE with a 6% gel and Coomassie stained. No bands were detected in the SDS washes after forty minutes for wild type and sixty minutes for *mdx*. Molecular weight markers (kDa) are indicated on the left.

Decellularization yield

To determine the decellularization yield, the wet weight of samples before and after decellularization was obtained (Table 1-1). While the average starting tissue weight for wild type samples was 404.6 mg, the average tissue remaining after decellularization was 25.9 mg, providing a yield of 6.4%. Due to fibrosis, *mdx* samples performed slightly better with an average pre-decellularization weight of 435.3 mg and a post- decellularization weight of 49.8 mg, for a yield of 12.0%.

Mass spectrometry detects significant changes in the mdx extracellular matrix

To determine the biochemical composition of the extracellular matrix, mass spectrometry was used to identify the digested peptides present in each sample. Although the samples were decellularized to remove the cellular material and enrich for matrix proteins, mass spectrometry analysis revealed that the decellularized matrix still retained many cellular proteins (Table 1-2). Most of these cellular proteins were of mitochondrial and cytoskeletal origin. Of the fifty-nine total identified proteins with a significant change between *mdx* vs. wild type, only twenty-five were matrisome or matrisome related proteins. These matrisome changes were from categories such as the collagens, glycoproteins, proteoglycans, regulators of the ECM, as well as ECM affiliated proteins (Table 1-3). The largest number of identified matrix changes came from the glycoproteins. While several types of collagen were identified, only collagen types I, III, and V were significantly upregulated in *mdx*. The only identified protein that was downregulated in *mdx* was EMILIN-3, a matrix glycoprotein.

Table 1-1: Pre- and post-decellularization wet weights

WT	Pre-decell (mg)	Post-decell (mg)	Yield (%)
1	406.4	28.4	7.0
2	403.9	15.1	3.7
3	403.4	34.2	8.5
Average	404.6	25.9	6.4

mdx	Pre-decell (mg)	Post-decell (mg)	Yield (%)
1	507.2	29.1	5.7
2	402.3	65.3	16.2
3	396.5	55.1	13.9
Average	435.3	49.8	12.0

Table 1-2: Identified proteins with a significant change between *mdx* vs. wild type quadricep muscle

	Protein	Gene Name	Uniprot ID	P-Value	Fold Change
	Dystrophin	DMD_MOUSE	P11531	7.50E-06	-15.36
*	EMILIN-3	EMIL3_MOUSE	P59900	0.01	-12.43
	Voltage-dependent anion-selective channel protein 1	VDAC1_MOUSE	Q60932	0.04	-3.43
	Complement decay-accelerating factor, GPI-anchored	DAF1_MOUSE	Q61475	0.04	-3.32
	CDGSH iron-sulfur domain-containing protein 1	CISD1_MOUSE	Q91WS0	0.04	-3.05
	NADH dehydrogenase [ubiquinone] flavoprotein 2, mitochondrial	NDUV2_MOUSE	Q9D6J6	0.03	-2.89
	Voltage-dependent anion-selective channel protein 3	VDAC3_MOUSE	Q60931	0.04	-2.83
	Keratin, type I cuticular Ha4	KRT34_MOUSE	Q9D646	0.02	-2.48
	Mitochondrial carrier homolog 2	MTCH2_MOUSE	Q791V5	0.04	-2.43
	NADH dehydrogenase [ubiquinone] 1 alpha subcomplex subunit 11	NDUAB_MOUSE	Q9D8B4	0.02	-2.43
	NADH dehydrogenase [ubiquinone] 1 beta subcomplex subunit 6	NDUB6_MOUSE	Q3UIU2	0.04	-2.20
	Myosin-8	MYH8_MOUSE	P13542	0.04	-2.19
	Myosin-11	MYH11_MOUSE	O08638	0.01	-2.13
	Cytochrome b-c1 complex subunit 2, mitochondrial	QCR2_MOUSE	Q9DB77	0.04	-2.10
	Microsomal glutathione S-transferase 3	MGST3_MOUSE	Q9CPU4	4.69E-03	-1.69
	ATP synthase subunit gamma, mitochondrial	ATPG_MOUSE	Q91VR2	0.03	-1.63
	Cytochrome c oxidase subunit NDUFA4	NDUA4_MOUSE	Q62425	0.04	-1.52
	Cytochrome b-c1 complex subunit 1, mitochondrial	QCR1_MOUSE	Q9CZ13	0.03	-1.46
	ATP synthase subunit epsilon, mitochondrial	ATP5E_MOUSE	P56382	0.04	-1.30
	NADH-ubiquinone oxidoreductase chain 1	NU1M_MOUSE	P03888	0.05	-1.29
	NADH dehydrogenase [ubiquinone] 1 alpha subcomplex subunit 2	NDUA2_MOUSE	Q9CQ75	0.04	-1.12
*	Nidogen-2	NID2_MOUSE	O88322	0.04	1.36
*	Collagen alpha-1(I) chain	CO1A1_MOUSE	P11087	8.85E-04	1.61
*	Collagen alpha-2(V) chain	CO5A2_MOUSE	Q3U962	0.01	1.76
*	Biglycan	PGS1_MOUSE	P28653	0.04	1.87
	Electron transfer flavoprotein subunit alpha, mitochondrial	ETFA_MOUSE	Q99LC5	0.04	2.15
	Complement C4-B	CO4B_MOUSE	P01029	0.02	2.20
*	Sushi repeat-containing protein SRPX2	SRPX2_MOUSE	Q8R054	0.01	2.21

*	Fibrinogen beta chain	FIBB_MOUSE	Q8K0E8	0.04	2.32
	Clusterin	CLUS_MOUSE	Q06890	0.04	2.39
*	Fibrinogen gamma chain	FIBG_MOUSE	Q8VCM7	0.04	2.41
	Galectin-1	LEG1_MOUSE	P16045	0.01	2.43
*	Inter-alpha-trypsin inhibitor heavy chain H2	ITIH2_MOUSE	Q61703	0.01	2.52
	Heterogeneous nuclear ribonucleoprotein K	HNRPK_MOUSE	P61979	0.04	2.56
*	Collagen alpha-1(V) chain	CO5A1_MOUSE	O88207	0.01	2.59
*	Fibronectin	FINC_MOUSE	P11276	0.01	2.78
*	Extracellular matrix protein 1	ECM1_MOUSE	Q61508	0.01	2.93
	40S ribosomal protein SA	RSSA_MOUSE	P14206	0.04	3.17
	Protein kinase C and casein kinase II substrate protein 3	PACN3_MOUSE	Q99JB8	0.04	3.25
	Antithrombin-III	ANT3_MOUSE	P32261	0.02	3.31
*	EMILIN-2	EMIL2_MOUSE	Q8K482	0.02	3.43
*	Kininogen-1	KNG1_MOUSE	O08677	0.03	3.70
*	Periostin	POSTN_MOUSE	Q62009	0.01	3.87
*	Collagen alpha-1(III) chain	CO3A1_MOUSE	P08121	0.01	3.88
*	Hemicentin-2	HMCN2_MOUSE	A2AJ76	8.68E-04	4.14
	Lipoprotein lipase	LIPL_MOUSE	P11152	0.01	4.69
*	Vitronectin	VTNC_MOUSE	P29788	0.01	4.98
	Eosinophil peroxidase	PERE_MOUSE	P49290	0.01	5.63
*	Bone marrow proteoglycan	PRG2_MOUSE	Q61878	0.02	6.08
*	Cartilage intermediate layer protein 1	CILP1_MOUSE	Q66K08	6.42E-04	7.88
*	Annexin A4	ANXA4_MOUSE	P97429	0.04	8.61
*	Cathepsin B	CATB_MOUSE	P10605	0.03	12.27
	Apolipoprotein E	APOE_MOUSE	P08226	0.01	13.75
*	Plasminogen	PLMN_MOUSE	P20918	0.02	14.04
	Prosaposin	SAP_MOUSE	Q61207	0.02	14.41
	Glia-derived nexin	GDN_MOUSE	Q07235	0.01	14.68
	40S ribosomal protein S11	RS11_MOUSE	P62281	0.04	14.70
*	Insulin-like growth factor-binding protein 7	IBP7_MOUSE	Q61581	0.02	15.46
*	Serine protease HTRA1	HTRA1_MOUSE	Q9R118	0.01	17.12

Table 1-3: Identified matrix proteins with a significant change between *mdx* vs. wild type quadricep muscle

Protein	Gene Name	Uniprot ID	P-Value	Fold Change
Collagens				
Collagen alpha-1(I) chain	CO1A1_MOUSE	P11087	8.85E-04	1.61
Collagen alpha-2(V) chain	CO5A2_MOUSE	Q3U962	0.01	1.76
Collagen alpha-1(V) chain	CO5A1_MOUSE	O88207	0.01	2.59
Collagen alpha-1(III) chain	CO3A1_MOUSE	P08121	0.01	3.88
Glycoproteins				
EMILIN-3	EMIL3_MOUSE	P59900	0.01	-12.43
Nidogen-2	NID2_MOUSE	O88322	0.04	1.36
Sushi repeat-containing protein SRPX2	SRPX2_MOUSE	Q8R054	0.01	2.21
Fibrinogen beta chain	FIBB_MOUSE	Q8K0E8	0.04	2.32
Fibrinogen gamma chain	FIBG_MOUSE	Q8VCM7	0.04	2.41
Fibronectin	FINC_MOUSE	P11276	0.01	2.78
Extracellular matrix protein 1	ECM1_MOUSE	Q61508	0.01	2.93
EMILIN-2	EMIL2_MOUSE	Q8K482	0.02	3.43
Periostin	POSTN_MOUSE	Q62009	0.01	3.87
Hemicentin-2	HMCN2_MOUSE	A2AJ76	8.68E-04	4.14
Vitronectin	VTNC_MOUSE	P29788	0.01	4.98
Cartilage intermediate layer protein 1	CILP1_MOUSE	Q66K08	6.42E-04	7.88
Insulin-like growth factor-binding protein 7	IBP7_MOUSE	Q61581	0.02	15.46
Proteoglycans				
Biglycan	PGS1_MOUSE	P28653	0.04	1.87
Bone marrow proteoglycan	PRG2_MOUSE	Q61878	0.02	6.08
ECM Regulators				
Inter-alpha-trypsin inhibitor heavy chain H2	ITIH2_MOUSE	Q61703	0.01	2.52
Kininogen-1	KNG1_MOUSE	O08677	0.03	3.70
Cathepsin B	CATB_MOUSE	P10605	0.03	12.27
Plasminogen	PLMN_MOUSE	P20918	0.02	14.04
Serine protease HTRA1	HTRA1_MOUSE	Q9R118	0.01	17.12
ECM Affiliated				
Annexin A4	ANXA4_MOUSE	P97429	0.04	8.61

Discussion

Through proteomics, many previously established matrisome changes were identified. These include the upregulation of collagen types I, III, V, periostin, and fibronectin in the *mdx* matrix [32-35]. While the increased abundance of these proteins has been well described, many less well known protein changes were also captured. Emilin-3 was the only matrisome component that was significantly downregulated in *mdx* mice. This matrix glycoprotein inhibits TGF-β signaling [36]. The TGF-β signaling pathway is involved in inflammation and is normally upregulated in response to skeletal muscle damage [37]. Therefore, downregulation of EMILIN-3 in the *mdx* matrix would relieve the inhibition on the TGF- β1 pathway [36], and potentially increase inflammation and deposition of fibrotic tissue. TGF- β1 upregulation also reduces the regenerative capacity of satellite cells by inhibiting their proliferation and differentiation [38]. Therefore, the observed downregulation of EMILIN-3 in *mdx* mice may play a role in DMD pathology.

There were also several proteins identified that have not been well described in the context of skeletal muscle. Extracellular matrix protein 1 (ECM1) is a matrix glycoprotein that binds to perlecan, a heperan sulfate proteoglycan that is an important component of the basement membrane through its role in cell proliferation and adhesion [39]. In skin, it is hypothesized that ECM1 acts as a "biological glue" that may interact with various growth factors and regulate the basement membrane [40, 41]. Mutations in ECM1 result in a disease known as lipoid proteinosis [40]. Of the many pathological features, notable ones include thickening of the basement membrane as well as easily damaged skin that leads to scarring [42]. It is hypothesized that the absence of ECM1 alters regulatory pathways that ultimately result in the overexpression of collagen type IV [42]. While we did not capture a change in collagen type IV in the current

analysis, it would be interesting to see whether the overexpression of ECM1 in *mdx* also results in reduced expression of collagen type IV in the dystrophic matrix. Whether this can be translated to the susceptibility of the sarcolemma to contraction-induced damage and resultant muscle fibrosis observed in DMD remains to be seen.

Insulin-like growth factor binding protein-7 (IGFBP-7) is another matrix glycoprotein that is significantly upregulated in the *mdx* matrix. It belongs to the larger IGFBP family that binds to insulin-like growth factors (IGF) and modulates various signaling pathways by regulating IGF activity [43-45]. While IGFBP-7 is known to be secreted by myoblasts, its exact role in skeletal muscle is poorly understood. In breast cancer cells, IGFBP-7 inhibited IGF-1 signaling and resulted in cellular apoptosis [46]. IGF-1 is especially relevant in the context of skeletal muscle as it is a major constituent of the IGF-1/AKT pathway that is involved with muscle growth [47]. If there is a similar mechanism in skeletal muscle, it may be possible that the significantly upregulated levels of IGFBP-7 in the *mdx* matrix also inhibits IGF-1 signaling and induces apoptosis of myocytes. Blocking IGFBP-7 expression may therefore be a potential therapeutic target for DMD.

The role of hemicentin-2 in vertebrate skeletal muscle remains poorly understood. Hemicentin-2 is a glycoprotein that is part of the fibulin family [48]. In C. elegans and zebrafish, hemicentin is capable of binding to perlecan in the basement membrane and may therefore be involved in the adhesion of the basement membranes between tissues [48, 49]. However, the cause of the significant upregulation of hemicentin-2 in *mdx* is not as readily apparent.

Although our initial screen of matrisome changes agrees with the previous literature, only twenty-five significant matrix changes were identified. This is a small fraction of the hundreds of proteins that exist in the extracellular matrix. Furthermore, the absence of laminin, perlecan, and

type IV collagen, major components of the basement membrane, asks the question of whether or not our protocol is sufficiently isolating and detecting matrix components [28]. Another challenge with the decellularization protocol is the drastically different decellularization times needed for wild type and *mdx* samples. It is plausible that the increased fibrosis observed in *mdx* samples may be hindering not only the removal of cellular material out of the matrix, but also the accessibility of the matrix to the digestive enzymes needed for mass spectrometry analysis and subsequent protein identification. Future sample preparations should involve a more rigorous disruption of the muscle to not only normalize the decellularization times between *mdx* and wild type, but also ensure that the proteins can be easily digested for mass spectrometry analysis.

One of the biggest challenges with the current decellularization protocol is a poor decellularization yield. Wild type and *mdx* samples had an average decellularization yield of 6.4% and 12.0% respectively due to a significant loss of tissue during the rinses to remove any remaining SDS and cellular debris. Furthermore, there was irreversible binding of the sample to the sides of the tubes used for decellularization which further lowered the decellularization yield. This was more pronounced for wild type rather than *mdx* samples. In addition, the increased fibrosis present in *mdx* mice correspondingly increased the yield. While low, this yield may be somewhat realistic as the extracellular matrix occupies only 10% of skeletal muscle by volume [50]. Furthermore, while collagen is the most abundant protein in the extracellular matrix, it only contributes 1-10% to the muscle dry weight [51-53]. This agrees with our yield data for wild type and *mdx* mice. However, the significant loss of decellularized tissue during the decellularization process needs to be addressed as the eventual goal of this protocol is to analyze limited quantities of human biopsies.

CHAPTER 2: PROTEOMIC ANALYSIS OF THE ECM WITH FRACTIONAL DECELLULARIZATION

Introduction

Although our previous method allowed for the successful detection of extracellular matrix proteins, very few matrisome changes were identified relative to the 274 proteins known to comprise the murine core matrisome [31]. To improve the detection of matrisome changes and to improve the removal of cellular contaminants, we utilized a fractionation based approach, allowing for isolation of specific muscle components. In addition, we explored the efficacy of homogenizing tissues to determine whether decellularization rates could be normalized between samples. We hypothesized that these protocol changes would increase the number of ECM protein changes identified through mass spectrometry.

Materials and Methods

Determining the effect of tissue homogenization

Tissue preparation

Quadricep muscles from eighteen to twenty-week-old wild type (n=1) and *mdx* mice (n=1) were obtained. For the proposed experiments, 100-200 mg of tissue was taken for each sample. Each sample was then homogenized using a chilled mortar and pestle before being stored at -80°C (Figure 2-1).

Time series decellularization

To assess the decellularization pattern of homogenized tissues, a time series decellularization was performed as previously described (page 6). Fractions were concentrated using Centriprep centrifugal filter units from EMD Millipore (Billerica, MA).

Confirmation of decellularization

The samples were then analyzed on a 7.5% SDS-PAGE gel that was cast using the SE600 Ruby Vertical Gel Unit from GE Healthcare Bio-Sciences (Pittsburgh, PA). A 7.5% separating/ 4% stacking gel was utilized to allow for improved separation of proteins on the larger gel. Fifty microliters from each time point were loaded with 1XLSB, and the gel was run overnight at 50mV. Visualization of the bands was performed as established before (page 7).

Mass spectrometry

Tissue preparation

Quadricep muscles from eighteen to twenty-week-old wild type (n=5) and *mdx* mice (n=5) were obtained. For the proposed experiments, 100-200 mg of tissue was taken for each sample. Each sample was then homogenized using a chilled mortar and pestle before being stored at -80°C (Figure 2-1).

Fractional decellularization

The fractional decellularization protocol performed was based on a previously described protocol by Naba et al [27]. The modified protocol utilized the compartmental protein extraction

kit from EMD Millipore (Billerica, MA). Homogenized samples were subjected to a series of buffers to extract the following fractions: (total tissue (TT), cytosolic (C), nuclear (N), membrane (M), cytoskeletal (CS), and a pellet that was enriched for the extracellular matrix (E). Ten micrograms of the pellet were removed from each sample for subsequent digestion, C18 tip cleanup, and analysis by mass spectrometry as described previously (pages 6-8).

Confirmation of decellularization

To determine whether the fractionated samples were adequately decellularized, the fractions were run on a 7.5% SDS-PAGE gel. Total tissue, cytosolic, nuclear, membrane, cytoskeletal fractions, and PBS rinses were mixed with 1x LSB containing 100mM DTT while the extracellular matrix fraction was mixed with 5x LSB containing 100mM DTT. Visualization of the bands was performed as established before (page 7).

Western Blotting

Proteins separated via SDS-PAGE were transferred onto nitrocellulose paper and visualized with Ponceau S staining. Following the transfer, the post-transferred SDS gel was stained with Coomassie Blue to confirm the successful transfer of proteins. Because changes in laminin in the *mdx* matrix were not detected in the previous protocol, the presence of laminin was probed to determine if there was an actual significant change between wild type and *mdx*, or if laminin was completely absent in the samples. To visualize the presence of laminin in each fraction, the nitrocellulose paper was incubated with an anti-laminin primary antibody (L9393, Sigma-Aldrich, concentration 1:1000), followed by the secondary antibody (ab6721, abcam, concentration 1:2000).

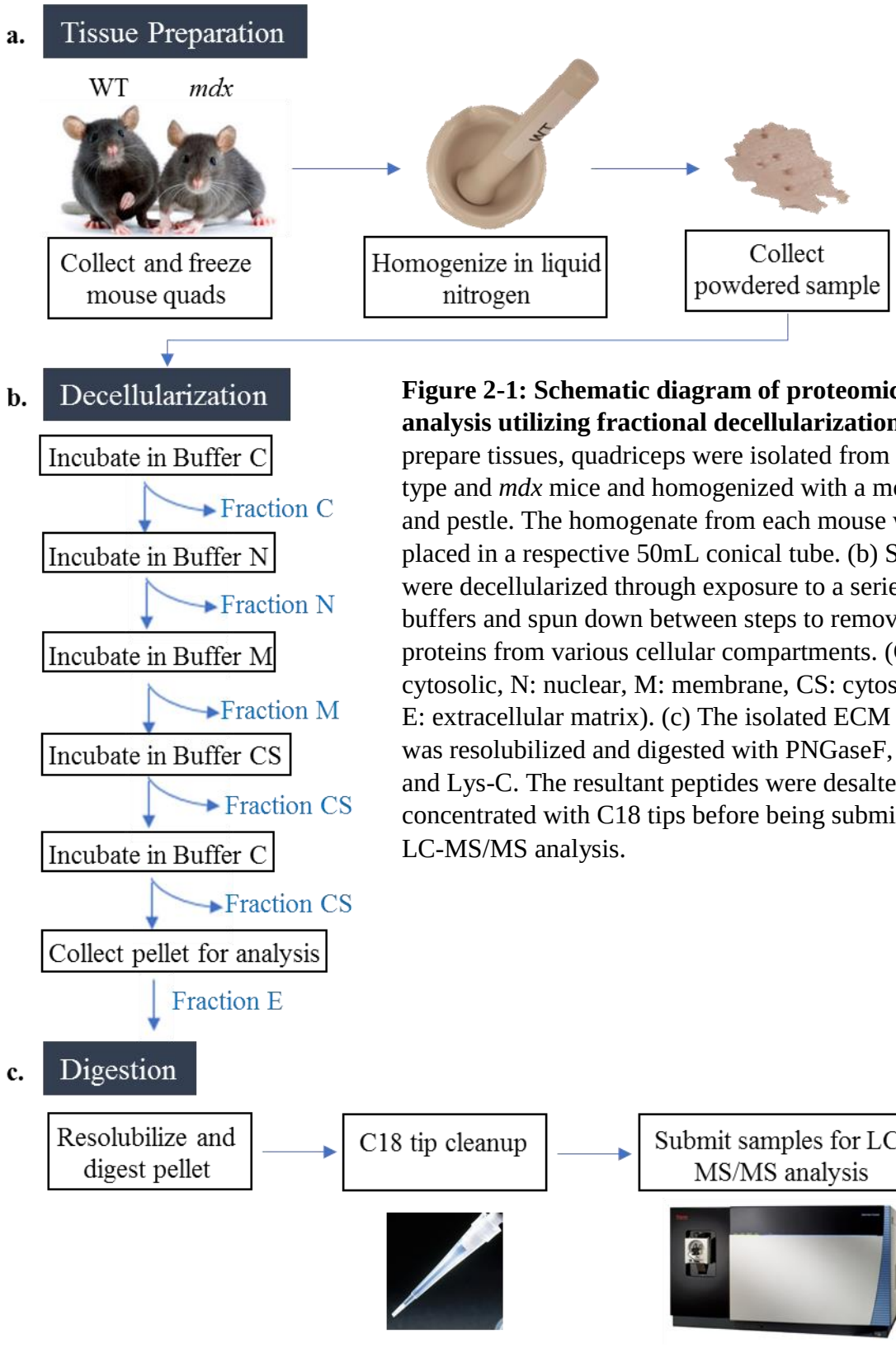

Figure 2-1: Schematic diagram of proteomic analysis utilizing fractional decellularization. (a) To prepare tissues, quadriceps were isolated from wild type and *mdx* mice and homogenized with a mortar and pestle. The homogenate from each mouse were placed in a respective 50mL conical tube. (b) Samples were decellularized through exposure to a series of buffers and spun down between steps to remove proteins from various cellular compartments. (C: cytosolic, N: nuclear, M: membrane, CS: cytoskeletal, E: extracellular matrix). (c) The isolated ECM pellet was resolubilized and digested with PNGaseF, trypsin, and Lys-C. The resultant peptides were desalted and concentrated with C18 tips before being submitted for LC-MS/MS analysis.

Results

Decellularization rate following homogenization

Time series decellularization of the homogenized tissue reveals that wild type and *mdx* muscles had a similar decellularization profile (Figure 2-2). Following SDS-PAGE and staining with Coomassie Blue, lightly stained bands were detected in both WT and *mdx* samples during the first twenty minutes of SDS rinses, with intense staining after fifty minutes. There is substantially more material loss at the later time points (fifty to seventy-minutes), which differs from the decellularization profile for sectioned tissues in which greater protein loss occurred during the first twenty-minutes.

Fractional decellularization greatly improves decellularization yield

The wet weight of samples before and after decellularization is presented in Table 2-1. Wild type samples had an average pre-decellularization (total tissue fraction) weight of 124 mg and a post-decellularization (extracellular matrix fraction) weight of 82mg for a decellularization yield of 66%. *Mdx* samples had an average pre-decellularization weight of 130 mg and a post-decellularization weight of 84mg for a decellularization yield of 65%.

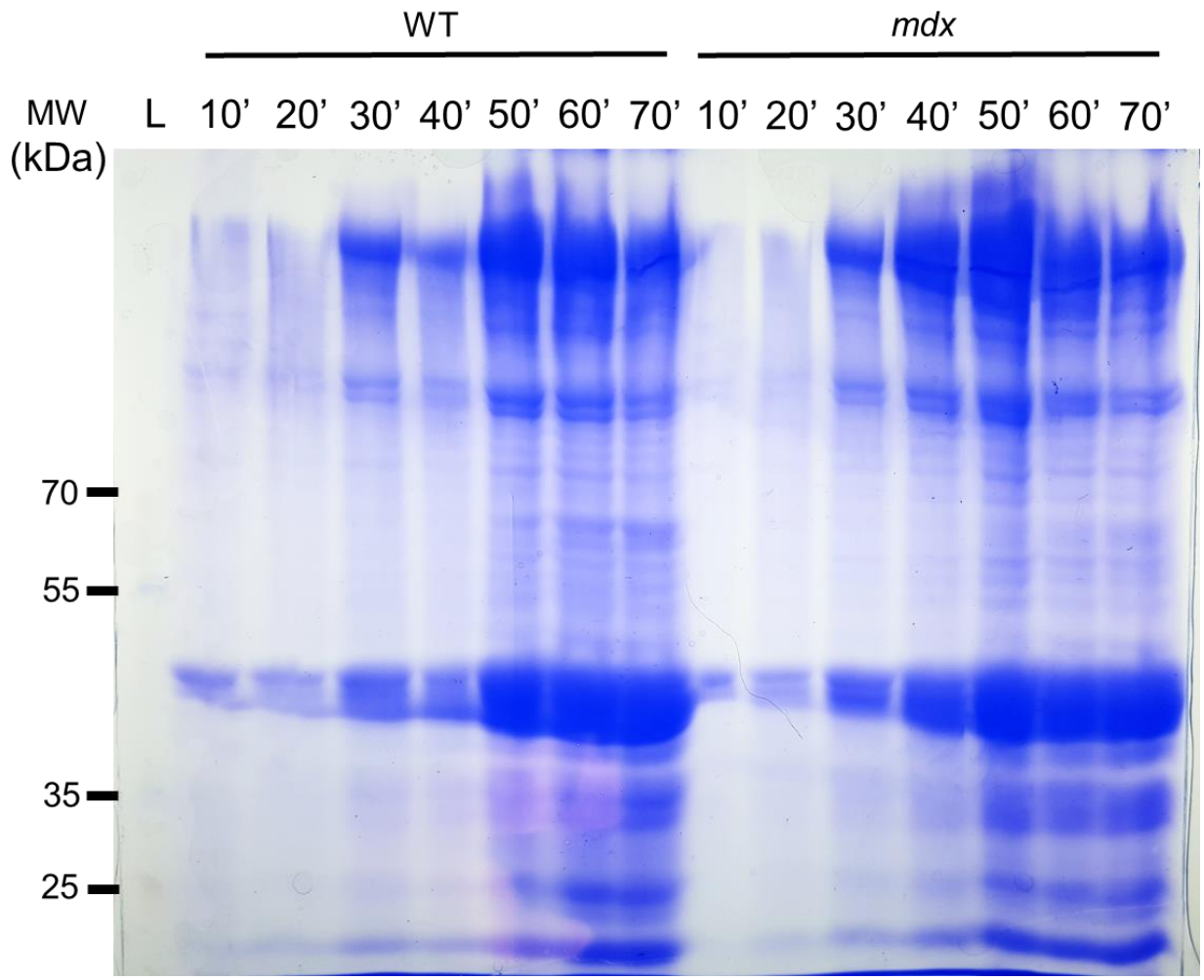

Figure 2-2: Homogenizing normalizes decellularization progress between wild type and *mdx*. Homogenized wild type (left) and *mdx* (right) samples were decellularized with fresh 1% SDS every ten minutes for seventy minutes. Ten-minute fractions were concentrated and analyzed through SDS-PAGE with a 7.5% gel. The bands were visualized with Coomassie Blue staining. Homogenizing improved decellularization by normalizing decellularization rates between wild type and *mdx* samples. Molecular weight markers (kDa) are indicated on the left.

Table 2-1: Pre- and post-decellularization wet weights

WT	Pre-decell (mg)	Post-decell (mg)	Yield (%)
1	130	84	65
2	130	89	69
3	130	75	58
4	130	82	63
5	102	78	76
Average	124	82	66

mdx	Pre-decell (mg)	Post-decell (mg)	Yield (%)
1	130	85	65
2	130	85	65
3	130	74	57
4	130	86	66
5	130	90	69
Average	130	84	65

Compartmental fractionation decellularization isolates different muscle fractions

To confirm that the compartmental protein extraction kit successfully decellularized the samples, a 7.5% SDS-PAGE gel was run (Figure 2-3). Total tissue fractions (TT) revealed a large number of bands with particularly strong staining around 250 and 40 kDa. Cytosolic (C), nuclear (N), membrane (M), and cytoskeletal (CS) fractions display different band profiles, confirming that different distributions of proteins are eluted in each fraction. The extracellular matrix fraction (E) displayed only two prominent bands at 250 and 40 kDa. It was noted that only the soluble proteins were able to run through the SDS-PAGE gel. Because the extracellular matrix consists largely of insoluble proteins, a majority of these were trapped at the bottom of the well and unable to enter through the stacking and separating gels. The lack of bands in the matrix fractions suggests the removal of cellular debris through each of the earlier fractions. Furthermore, the decrease in band intensity of the 250 and 40kDa bands from the total tissue to the matrix fractions suggests an enrichment for the extracellular matrix and therefore suggests that decellularization occurred.

Mass Spectrometry

One hundred total significant changes between *mdx* and wild type decellularized tissues were identified from mass spectrometry (Table 2-2). Of these total hits, only eleven were matrisome or matrisome-associated proteins (Table 2-3). Many of the cellular contaminants included contractile proteins such as myosin, as well as mitochondrial proteins. The largest group of identified proteins belonged to the glycoproteins. Laminin β1 and α4 were significantly upregulated in the *mdx* matrix compared to wild type. Thrombospondin-4, asporin, and lumican

were detected, something not observed in the previous protocol. Periostin, fibronectin, and cartilage intermediate protein 1 (CILP1) were identified as significantly upregulated in *mdx.*

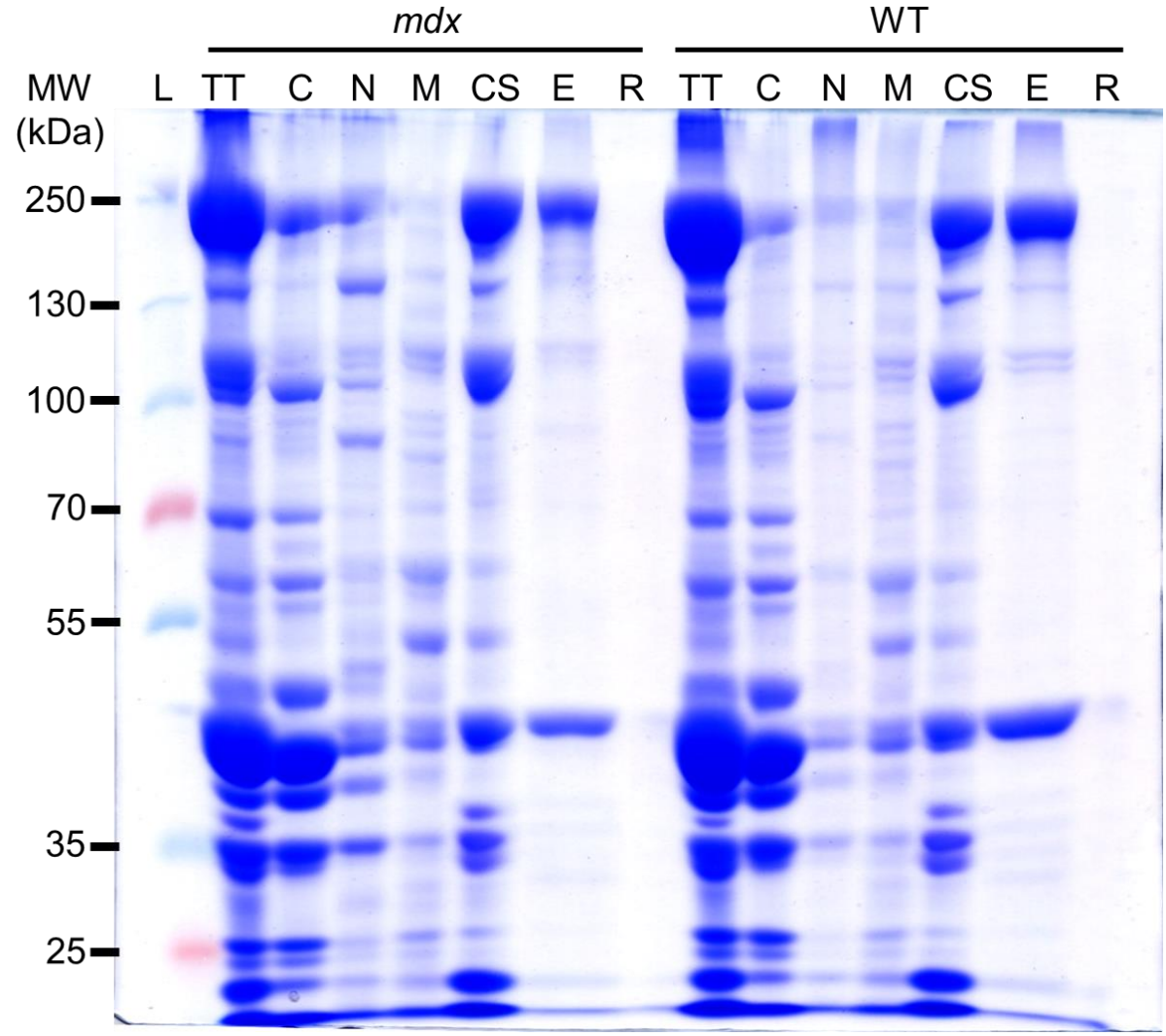

Figure 2-3: Compartmental protein extraction isolates muscle fractions. *Mdx* (left) and wild type (right) samples were decellularized utilizing EMD Millipore's compartmental protein extraction kit. A series of buffers were used to extract cytosolic, nuclear, membrane, cytoskeletal, and extracellular matrix proteins from the total tissue extract. Protein fractions were analyzed through SDS-PAGE with a 7.5% gel. The bands were visualized with Coomassie Brilliant Blue staining. (L: ladder, TT: total tissue, C: cytosolic, N: nuclear, M: membrane, CS: cytoskeletal, E: extracellular matrix, R: PBS rinse). Wild type and *mdx* matrix fractions both showed a vast removal of proteins from the total tissue fraction, enriching for insoluble extracellular matrix proteins that are unable to run through the gel. Molecular weight markers (kDa) are indicated on the left.

Table 2-2: Identified proteins with a significant change between *mdx* vs. wild type quadricep muscle

Protein	Gene Name	UNIPROT ID	P-Value	Fold Change
Dystrophin	DMD_MOUSE	P11531	0.00	-21.14
D-beta-hydroxybutyrate dehydrogenase, mitochondrial	BDH_MOUSE	Q80XN0	0.02	-12.18
Ankyrin repeat and SOCS box protein 2	ASB2_MOUSE	Q8K0L0	0.02	-11.04
Myeloid leukemia factor 1	MLF1_MOUSE	Q9QWV4	0.02	-7.83
Perilipin-4	PLIN4_MOUSE	O88492	0.03	-6.67
Alpha-1-syntrophin	SNTA1_MOUSE	Q61234	0.02	-6.07
Cytochrome b-c1 complex subunit 8	QCR8_MOUSE	Q9CQ69	0.03	-4.74
Mitochondrial pyruvate carrier 2	MPC2_MOUSE	Q9D023	0.00	-4.29
NADH dehydrogenase [ubiquinone] 1 alpha subcomplex subunit 7	NDUA7_MOUSE	Q9Z1P6	0.01	-3.59
Keratin, type II cytoskeletal 1	K2C1_MOUSE	P04104	0.01	-3.24
Lipoamide acyltransferase component of branched-chain alpha-keto acid dehydrogenase complex, mitochondrial	ODB2_MOUSE	P53395	0.01	-3.12
Acyl-coenzyme A thioesterase 13	ACO13_MOUSE	Q9CQR4	0.03	-2.07
Parvalbumin alpha	PRVA_MOUSE	P32848	0.01	-2.00
PDZ and LIM domain protein 5	PDLI5_MOUSE	Q8CI51	0.02	-1.95
Glycerol-3-phosphate dehydrogenase, mitochondrial	GPDM_MOUSE	Q64521	0.01	-1.65
Sulfide:quinone oxidoreductase, mitochondrial	SQRD_MOUSE	Q9R112	0.00	-1.58
Succinate dehydrogenase [ubiquinone] iron-sulfur subunit, mitochondrial	SDHB_MOUSE	Q9CQA3	0.01	-1.52
F-actin-capping protein subunit alpha-2	CAZA2_MOUSE	P47754	0.00	-1.47
Myosin-binding protein C, fast-type	MYPC2_MOUSE	Q5XKE0	0.00	-1.37
NADH dehydrogenase [ubiquinone] 1 alpha subcomplex subunit 9, mitochondrial	NDUA9_MOUSE	Q9DC69	0.00	-1.28
Histone-lysine N-methyltransferase Smyd1	SMYD1_MOUSE	P97443	0.00	-1.24
Myozenin-1	MYOZ1_MOUSE	Q9JK37	0.02	-1.21
Calcium/calmodulin-dependent protein kinase type II subunit alpha	KCC2A_MOUSE	P11798	0.00	-1.17
Motile sperm domain-containing protein 1	MSPD1_MOUSE	Q8VEL0	0.03	-1.13

	LIM domain-binding protein 3	LDB3_MOUSE	Q9JKS4	0.02	-1.06
	Cytochrome b-c1 complex subunit 6, mitochondrial	QCR6_MOUSE	P99028	0.00	-1.05
	Cytochrome c1, heme protein, mitochondrial	CY1_MOUSE	Q9D0M3	0.04	-1.03
	ATP synthase subunit d, mitochondrial	ATP5H_MOUSE	Q9DCX2	0.02	-1.02
	NADH dehydrogenase [ubiquinone] iron-sulfur protein 4, mitochondrial	NDUS4_MOUSE	Q9CXZ1	0.00	-1.01
	Transmembrane emp24 domain-containing protein 10	TMEDA_MOUSE	Q9D1D4	0.03	1.07
	40S ribosomal protein S14	RS14_MOUSE	P62264	0.02	1.15
	Histone H4	H4_MOUSE	P62806	0.01	1.16
	40S ribosomal protein S9	RS9_MOUSE	Q6ZWN5	0.00	1.18
	40S ribosomal protein S16	RS16_MOUSE	P14131	0.03	1.20
	Ras-related protein Rab-10	RAB10_MOUSE	P61027	0.00	1.23
*	Asporin	ASPN_MOUSE	Q99MQ4	0.02	1.28
	Mast cell carboxypeptidase A	CBPA3_MOUSE	P15089	0.02	1.36
	Polymerase I and transcript release factor	PTRF_MOUSE	O54724	0.01	1.45
	Stromal interaction molecule 1	STIM1_MOUSE	P70302	0.01	1.45
	Kelch-like protein 40	KLH40_MOUSE	Q9D783	0.00	1.48
	Plasma membrane calcium-transporting ATPase 1	AT2B1_MOUSE	G5E829	0.01	1.50
*	Laminin subunit beta-1	LAMB1_MOUSE	P02469	0.00	1.65
	60S ribosomal protein L10a	RL10A_MOUSE	P53026	0.05	1.67
	Starch-binding domain-containing protein 1	STBD1_MOUSE	Q8C7E7	0.00	1.73
	Kinectin	KTN1_MOUSE	Q61595	0.03	1.84
	Gelsolin	GELS_MOUSE	P13020	0.00	1.95
	Myomesin-3	MYOM3_MOUSE	A2ABU4	0.00	2.11
	Mitochondrial import receptor subunit TOM22 homolog	TOM22_MOUSE	Q9CPQ3	0.03	2.13
	Integrin alpha-7	ITA7_MOUSE	Q61738	0.00	2.37
*	Lumican	LUM_MOUSE	P51885	0.03	2.48
	Prelamin-A/C	LMNA_MOUSE	P48678	0.00	2.49
	NADH-cytochrome b5 reductase 3	NB5R3_MOUSE	Q9DCN2	0.04	2.73

	Vimentin	VIME_MOUSE	P20152	0.00	3.25
	Elongation factor 2	EF2_MOUSE	P58252	0.00	3.48
	PRA1 family protein 3	PRAF3_MOUSE	Q8R5J9	0.03	3.49
	Electron transfer flavoprotein subunit beta	ETFB_MOUSE	Q9DCW4	0.03	3.63
	Calpain-1 catalytic subunit	CAN1_MOUSE	O35350	0.04	3.84
*	Thrombospondin-4	TSP4_MOUSE	Q9Z1T2	0.00	5.07
	Muscle-related coiled-coil protein	MURC_MOUSE	A2AMM0	0.03	6.54
	Spectrin beta chain, non-erythrocytic 1	SPTB2_MOUSE	Q62261	0.02	6.61
	FH1/FH2 domain-containing protein 1	FHOD1_MOUSE	Q6P9Q4	0.04	6.86
	Heat shock protein beta-7	HSPB7_MOUSE	P35385	0.04	7.38
	Calcium uniporter protein, mitochondrial	MCU_MOUSE	Q3UMR5	0.02	7.55
	26S protease regulatory subunit 8	PRS8_MOUSE	P62196	0.05	7.65
	Protein kinase C and casein kinase II substrate protein 3	PACN3_MOUSE	Q99JB8	0.02	7.88
	Elongation factor 1-beta	EF1B_MOUSE	O70251	0.00	8.02
	40S ribosomal protein SA	RSSA_MOUSE	P14206	0.01	8.04
*	Annexin A2	ANXA2_MOUSE	P07356	0.02	8.15
	1-acyl-sn-glycerol-3-phosphate acyltransferase gamma	PLCC_MOUSE	Q9D517	0.04	8.29
*	Laminin subunit alpha-4	LAMA4_MOUSE	P97927	0.03	8.34
	Unconventional myosin-Ic	MYO1C_MOUSE	Q9WTI7	0.02	8.68
	Heterogeneous nuclear ribonucleoprotein M	HNRPM_MOUSE	Q9D0E1	0.03	8.92
	60S ribosomal protein L3	RL3_MOUSE	P27659	0.00	8.99
	Myosin light chain 4	MYL4_MOUSE	P09541	0.04	9.00
	Myosin light chain 6B	MYL6B_MOUSE	Q8CI43	0.01	9.61
	Isoleucine--tRNA ligase, cytoplasmic	SYIC_MOUSE	Q8BU30	0.02	10.21
	Beta-2-glycoprotein 1	APOH_MOUSE	Q01339	0.03	10.71
	40S ribosomal protein S3	RS3_MOUSE	P62908	0.03	10.75
	SUN domain-containing protein 2	SUN2_MOUSE	Q8BJS4	0.02	10.82
	Glutathione peroxidase 1	GPX1_MOUSE	P11352	0.05	11.34

	Transmembrane protein 43	TMM43_MOUSE	Q9DBS1	0.02	11.56
	Sideroflexin-3	SFXN3_MOUSE	Q91V61	0.01	11.60
	Major vault protein	MVP_MOUSE	Q9EQK5	0.00	11.72
	Protein NDRG2	NDRG2_MOUSE	Q9QYG0	0.02	11.87
	Manganese-transporting ATPase 13A1	AT131_MOUSE	Q9EPE9	0.00	12.03
	Lamin-B2	LMNB2_MOUSE	P21619	0.01	12.19
	Myosin-9	MYH9_MOUSE	Q8VDD5	0.00	12.73
	T-complex protein 1 subunit beta	TCPB_MOUSE	P80314	0.02	13.25
*	Serpin B6	SPB6_MOUSE	Q60854	0.01	14.35
*	Annexin A11	ANX11_MOUSE	P97384	0.00	15.04
	Clusterin	CLUS_MOUSE	Q06890	0.00	16.60
	Receptor of activated protein C kinase 1	RACK1_MOUSE	P68040	0.00	16.66
	Filamin-A	FLNA_MOUSE	Q8BTM8	0.00	16.99
*	Periostin	POSTN_MOUSE	Q62009	0.00	17.30
	Eosinophil peroxidase	PERE_MOUSE	P49290	0.00	17.72
*	Fibronectin	FINC_MOUSE	P11276	0.00	17.99
	Extended synaptotagmin-1	ESYT1_MOUSE	Q3U7R1	0.00	18.38
	Myosin-3	MYH3_MOUSE	P13541	0.00	19.47
	NAD(P) transhydrogenase, mitochondrial	NNTM_MOUSE	Q61941	0.00	20.02
*	Cartilage intermediate layer protein 1	CILP1_MOUSE	Q66K08	0.00	21.64

Table 2-3: Identified matrix proteins with a significant change between *mdx* vs. wild type quadricep muscle

Protein	Gene Name	Uniprot ID	P-Value	Fold Change
Glycoproteins				
Laminin subunit beta-1	LAMB1_MOUSE	P02469	0.00	1.65
Thrombospondin-4	TSP4_MOUSE	Q9Z1T2	0.00	5.07
Laminin subunit alpha-4	LAMA4_MOUSE	P97927	0.03	8.34
Periostin	POSTN_MOUSE	Q62009	0.00	17.30
Fibronectin	FINC_MOUSE	P11276	0.00	17.99
Cartilage intermediate layer protein 1	CILP1_MOUSE	Q66K08	0.00	21.64
Proteoglycans				
Asporin	ASPN_MOUSE	Q99MQ4	0.02	1.28
Lumican	LUM_MOUSE	P51885	0.03	2.48
Matrisome-associated				
Annexin A2	ANXA2_MOUSE	P07356	0.02	8.15
Serpin B6	SPB6_MOUSE	Q60854	0.01	14.35
Annexin A11	ANX11_MOUSE	P97384	0.00	15.04

Western Blotting

To determine the cause for the low number of changes detected by mass spectrometry, Western Blotting was performed on the fractionated samples. Not all of the bands present in each fraction were efficiently transferred to the nitrocellulose membrane (Figure 2-4). Ponceau S staining of the membrane and Coomassie staining of the post-transferred gel revealed less intense staining for bands greater than 100kDa and less than 35kDa. Bands of approximately 250kDa were especially difficult to transfer to the membrane. One of the significant changes detected during mass spectrometry, laminin, was chosen to understand which fraction it eluted from during the fractionation protocol. Western Blotting showed that laminin was detected in every fraction for both wild type and *mdx* (Figure 2-5), with the exception of the membrane fraction for *mdx* which possibly resulted from an error in loading the original sample. Furthermore, there is a poor enrichment for laminin in the extracellular matrix fraction. Instead, it appears laminin is non-selectively removed at each step of the fractionation protocol and appears in the nuclear and cytoskeletal fractions just as prominently as the matrix fractions.

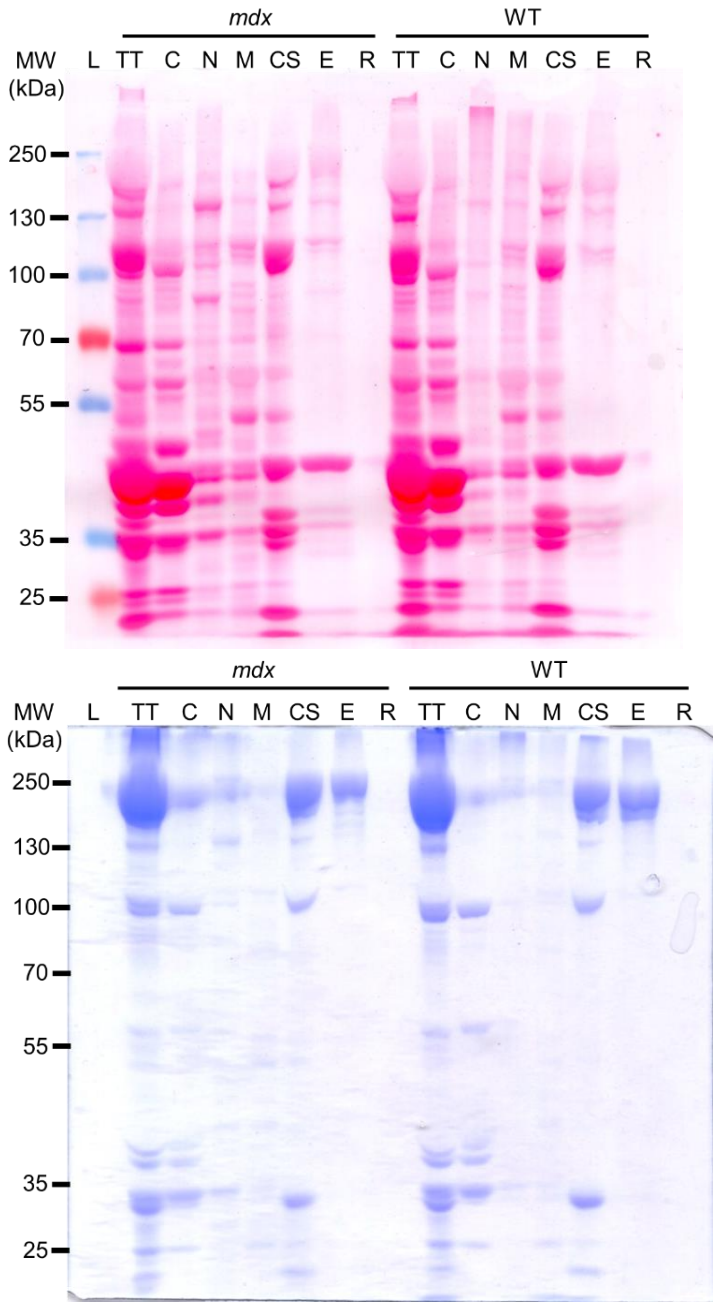

Figure 2-4: Not all proteins are efficiently transferred to the nitrocellulose membrane. (a) *Mdx* (left) and wild type (right) samples decellularized with EMD Millipore's compartmental protein extraction kit, run through SDS-PAGE, and transferred onto nitrocellulose paper. Transferred bands were visualized with Ponceau S staining. (L: ladder, TT: total tissue, C: cytosolic, N: nuclear, M: membrane, CS: cytoskeletal, ECM: extracellular matrix, R: PBS rinse.) (b) The post-transferred gel was Coomassie stained to determine transfer efficiency. Bands greater than 100 kDa, especially at 250 kDa, and bands lower than 35 kDa were not completely transferred to the nitrocellulose membrane. Molecular weight markers (kDa) are indicated on the left.

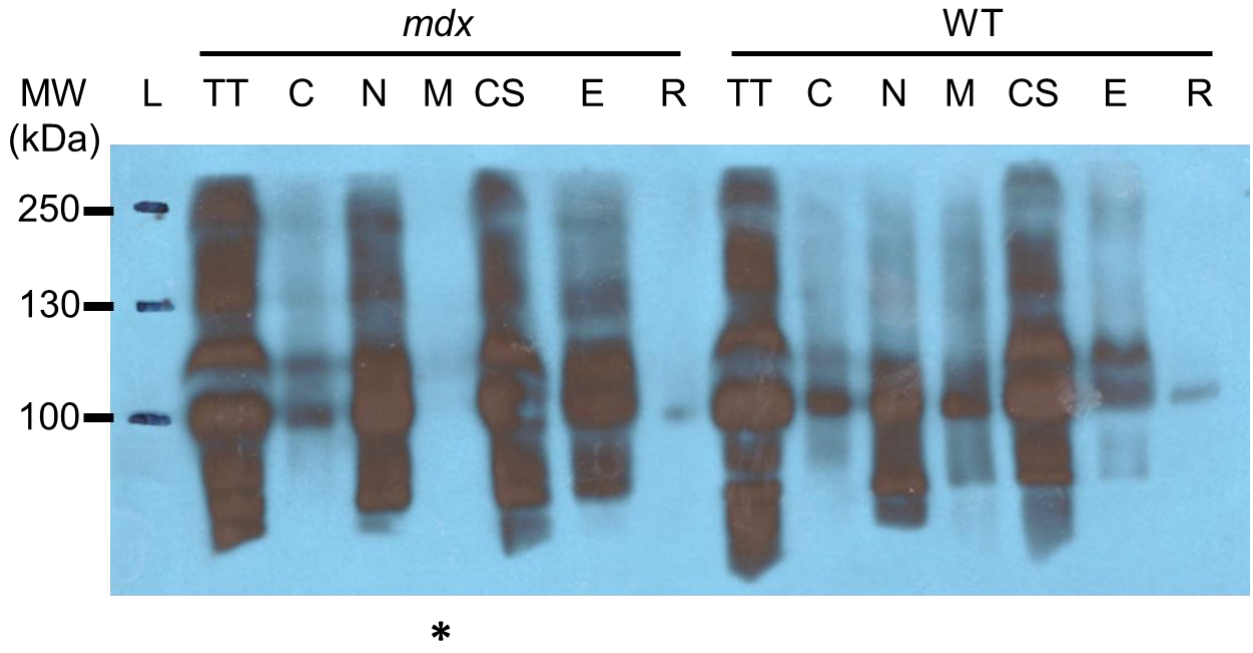

Figure 2-5: Laminin is present in each fraction. *Mdx* (left) and wild type (right) samples were decellularized with EMD Millipore's compartmental protein extraction kit, run through SDS-PAGE, and transferred onto nitrocellulose paper. Laminin was present in every fraction for both *mdx* and wild type with the exception of the membrane fraction for *mdx.* Laminin, a matrisome protein, was especially present in the nuclear, cytoskeletal, and extracellular matrix fractions. Due to extensive laminin loss in fractions other than the matrix fraction, fractionation is a poor method for enrichment of laminin. L: ladder, TT: total tissue, C: cytosolic, N: nuclear, M: membrane, CS: cytoskeletal, ECM: extracellular matrix, R: PBS rinse. * represents possible loading error during SDS-PAGE. Molecular weight markers (kDa) are indicated on the left.

Discussion

One of the advantages of the fractionation protocol was the use of homogenization. When compared to decellularizing sectioned tissue, decellularizing homogenized tissue increases the ability of SDS to remove proteins from the matrix over time. For a similar starting pre-decellularization weight, both wild type and *mdx* ended up with similar post-decellularization weights, confirming that homogenizing tissues prior to decellularization normalizes the decellularization rates between wild type and *mdx*. Therefore, homogenization improved the treatment protocol by establishing a single time for decellularization and allowed a greater degree of consistency between samples.

Although it was expected that decellularization with the compartmental protein kit would increase the number of matrisome changes, mass spectrometry analysis of the extracellular matrix fraction produced fewer hits than with analysis of the decellularized sectioned tissues. Of the 100 total significant changes between *mdx* and wild type, only 11 were matrisome proteins. This is drastically different from the previous chapter where we identified 59 total significant changes between *mdx* and wild type, of which 25 were identified as components of the matrisome. While the previous protocol identified several collagens, the fractionation protocol identified no significant differences in collagens. Furthermore, several proteins identified before were absent from this round of mass spectrometry. Despite fractionating the samples, large amounts of cellular contaminates such as mitochondrial proteins and myosin still appeared in the matrix fractions.

Given the high tissue yield following the fractional decellularization protocol, we expected to detect many more matrix proteins. The yields for both wild type and *mdx* was 66%

and 65% respectively, were nearly eleven times greater for wild type and five times greater for *mdx* than the yields observed when decellularizing with SDS. However, these yields are higher than would be expected since the matrix is only 1-10% of the total tissue by dry weight. The high yield may be a result of insufficient decellularization which would explain the large number of muscle proteins changes and low number of matrisome changes. In addition, the fractionation protocol did not seem to result in the correct proteins being extracted in their appropriate cellular fractions. Laminin staining revealed laminin present not only in the matrix fraction, but in all the fractions. If other matrix proteins are being extracted at earlier fractions and are not fully retained in the extracellular matrix, it is not possible to accurately quantitate matrisome changes between *mdx* and wild type.

Considering that glycoproteins make up a relatively small fraction of the matrisome compared to structural proteins such as collagen, the inability to retain matrix components through fractionation makes it even more difficult to detect these small changes. Using the same fractions produced by this protocol, other members of our lab have stained for various sarcolemmal and cytosolic proteins and have noted that these proteins of interest end up in more than just the fractions they are expected to be found in. The buffers in the compartmental protein extraction kit do not seem to be able to cleanly extract for proteins by compartment and fractionation is therefore not an effective method to enrich for extracellular matrix proteins. While Naba and colleagues [28] had success with the fractionation protocol, this may be due to the choice of tissues they used, carcinoma and diaphragm. These two tissues are very different from skeletal muscle and are expected to have much less contractile proteins. It may be unrealistic to sufficiently remove these cellular contaminants in skeletal muscle to unmask all of the biological changes that are occurring between *mdx* and wild type. Due to this difficulty, a

future direction may be to remove the cellular contaminants from the spectral data before running the statistical analysis.

Despite these shortcomings, the fractionation protocol was still able to identify the upregulation of laminin, an important component of the basement membrane that we had previously not been able to detect, as a significant change between *mdx* and wild type. Furthermore, periostin and fibronectin showed up again as major changes in the *mdx* matrix. Another glycoprotein, cartilage intermediate protein 1 appeared as the largest change in the *mdx* matrix. While we observed this change in the previous mass spectrometry protocol, we had dismissed its importance, as it appeared to be a glycoprotein that was more relevant in chondrocytes. Although CILP1 is more thoroughly studied in the context of cartilage, it has been found to be expressed in other tissues such as heart and skeletal muscle [54]. In degenerative conditions such as aging and osteoarthritis, CILP1 expression can be induced by TGF-beta signaling in cartilaginous tissue, which subsequently inhibits IGF-1 signaling and reduces cellular proliferation [55]. Although TGF-beta signaling initially induces the expression of CILP1, high CILP1 levels in turn inhibit TGF-beta signaling in cardiac fibroblasts through a negative feedback loop and block their differentiation into myofibroblasts [56]. While CILP1 is constantly involved with general homeostasis in cartilaginous tissues, CILP1 is only expressed after injury in cardiac muscle [56]. The significant increase in CILP1 in the *mdx* matrix is therefore puzzling as high expression of CILP1 should reduce TGF-beta signaling and ameliorate the fibrosis observed [37]. Because myocardial infarction is an acute injury, the high levels of CILP1 in *mdx* may be due to dysregulation of the TGF-beta signaling cascade and negative feedback loop due to chronic inflammation and injury in DMD [56]. Further research into this altered cascade may provide clues to the cause of the aberrant signaling.

CONCLUSION

Through proteomic analysis of the extracellular matrix of dystrophic and wild type mice, we were able to identify several proteins that are upregulated and downregulated in the matrix in DMD. These not only captured previously established changes such as fibronectin, periostin, and various collagens, but also proteins that are not so well known in the context of DMD such as EMILIN-3, ECM1, CILP1, and HMCN1. We compared two protocols to decellularize and analyze the matrix through mass spectrometry. In the first method, we found that sectioning the tissues and decellularizing with SDS resulted in low decellularization yield. In the second method, homogenizing tissue and fractionation improved the decellularization yield but resulted in a greater number of cellular contaminants which obscured many matrisome changes. Future studies will aim to combine these two protocols, utilizing the homogenization from the fractionation protocol, but decellularizing with SDS instead of the fractionation protocol. While previous attempts in our lab have failed using homogenized tissue for SDS decellularization and subsequent mass spectrometry analysis, this is most likely due to improper times of decellularization that resulted in too much sample loss.

The importance of utilizing proteomics to study how the matrix changes in DMD is paramount as it allows a broader identification of proteins than would be possible through Western Blotting alone. Identification of these changes may elucidate additional biomarkers for DMD as well as the discovery of novel therapeutic targets. Future directions will examine: 1) whether human samples display similar matrisome changes as *mdx*, and 2) whether the inflammatory process and subsequent matrix remodeling by acute damage through cardiotoxin injections is different in *mdx.*

REFERENCES

[1] Hor, K.N., Taylor, M.D., Al-Khalidi, H.R., Cripe, L.H., Raman, S.V., Jefferies, J.L., . . . Mazur, W. (2013). Prevalence and distribution of late gadolinium enhancement in a large population of patients with Duchenne muscular dystrophy: effect of age and left ventricular systolic function. Journal of Cardiovascular Magnetic Resonance, 15(1), 107. doi:10.1186/1532-429X-15-107

[2] Kharraz, Y., Guerra, J., Pessina, P., Serrano, A. L., Muñoz-Cánoves, P. (2014). Understanding the Process of Fibrosis in Duchenne Muscular Dystrophy. BioMed Research International, 2014, 1-11. doi:10.1155/2014/965631

[3] Zanotti, S., Bragato, C., Zucchella, A., Maggi, L., Mantegazza, R., Morandi, L., Mora, M. (2016). Anti-fibrotic effect of pirfenidone in muscle derived-fibroblasts from Duchenne muscular dystrophy patients. Life Sciences, 145, 127-136. doi:10.1016/j.lfs.2015.12.015

[4] Aliverti, A., Lomauro, A., Dangelo, M. G. (2015). Assessment and management of respiratory function in patients with Duchenne muscular dystrophy: current and emerging options. Therapeutics and Clinical Risk Management, 11, 1475-1488. doi:10.2147/tcrm.s55889

[5] Konieczny, P., Swiderski, K., Chamberlain, J.S. (2013). Gene and cell-mediated therapies for muscular dystrophy. Muscle & Nerve, 47(5), 649-663. doi:10.1002/mus.23738

[6] Goudenege, S., Lamarre, Y., Dumont, N., Rousseau, J., Frenette, J., Skuk, D., Tremblay, J. P. (2010). Laminin-111: A Potential Therapeutic Agent for Duchenne Muscular Dystrophy. Molecular Therapy, 18(12), 2155-2163. doi:10.1038/mt.2010.165

[7] Irintchev, A., Rosenblatt, J.D., Cullen, M.J., Zweyer, M., Wernig, A. (1998). Ectopic skeletal muscles derived from myoblasts implanted under the skin. Journal of Cell Science, 111(22),3287–3297.

[8] Nishimura, T. (2015). Role of extracellular matrix in development of skeletal muscle and postmortem aging of meat. Meat Science, 109, 48-55. doi:10.1016/j.meatsci.2015.05.015

[9] Kishioka, Y., Thomas, M., Wakamatsu, J., Hattori, A., Sharma, M., Kambadur, R., Nishimura, T. (2008). Decorin enhances the proliferation and differentiation of myogenic cells through suppressing myostatin activity. Journal of Cellular Physiology, 215(3), 856-867. doi:10.1002/jcp.21371

[10] Li, Z.B., Kollias, H.D., Wagner, K.R. (2008). Myostatin Directly Regulates Skeletal Muscle Fibrosis. Journal of Biological Chemistry, 283(28), 19371-19378. doi:10.1074/jbc.m802585200

[11] Streuli, C.H., Schmidhauser, C., Kobrin, M., Bissell, M.J., Derynck, R. (1993). Extracellular matrix regulates expression of the TGF-beta 1 gene. The Journal of Cell Biology, 120(1), 253-260. doi:10.1083/jcb.120.1.253

[12] Hyytiäinen, M., Penttinen, C., Keski-Oja, J. (2004). Latent TGF-β Binding Proteins: Extracellular Matrix Association and Roles in TGF-β Activation. Critical Reviews in Clinical Laboratory Sciences, 41(3), 233-264. doi:10.1080/10408360490460933

[13] Yu, Q., Stamenkovic, I. (2000). Cell surface-localized matrix metalloproteinase-9 proteolytically activates TGF-β and promotes tumor invasion and angiogenesis. Genes & Development, 14(2):163-176.

[14] Murphy-Ullrich, J.E., Poczatek, M. (2000). Activation of latent TGF-β by thrombospondin-1: mechanisms and physiology. Cytokine & Growth Factor Reviews, 11(1-2), 59-69. doi:10.1016/s1359-6101(99)00029-5

[15] Munger, J.S., Huang, X., Kawakatsu, H., Griffiths, M.J., Dalton, S. L., Wu, J., . . . Sheppard, D. (1999). A Mechanism for Regulating Pulmonary Inflammation and Fibrosis: The Integrin αvβ6 Binds and Activates Latent TGF β1. Cell, 96(3), 319-328. doi:10.1016/s0092-8674(00)80545-0

[16] Worthington, J.J., Klementowicz, J.E., Travis, M.A. (2011). TGFβ: a sleeping giant awoken by integrins. Trends in Biochemical Sciences, 36(1), 47-54. doi:10.1016/j.tibs.2010.08.002

[17] Lyons, R.M., Keski-Oja, J., Moses, H.L. (1988). Proteolytic activation of latent transforming growth factor-beta from fibroblast-conditioned medium. The Journal of Cell Biology,106(5), 1659-1665. doi:10.1083/jcb.106.5.1659

[18] Vo, A. H., & Mcnally, E. M. (2015). Modifier genes and their effect on Duchenne muscular dystrophy. Current Opinion in Neurology, 28(5), 528-534. doi:10.1097/wco.0000000000000240

[19] Mukund, K., Subramaniam, S. (2015). Dysregulated mechanisms underlying Duchenne muscular dystrophy from co-expression network preservation analysis. BMC Research Notes, 8(1), 182. doi:10.1186/s13104-015-1141-9

[20] Vidal, B., Ardite, E., Suelves, M., Ruiz-Bonilla, V., Janué, A., Flick, M.J., . . . Muñoz-Cánoves, P. (2012). Amelioration of Duchenne muscular dystrophy in mdx mice by elimination of matrix-associated fibrin-driven inflammation coupled to the αMβ2 leukocyte integrin receptor. Human Molecular Genetics,21(9), 1989-2004. doi:10.1093/hmg/dds012

[21] Turgeman, T., Hagai, Y., Huebner, K., Jassal, D.S., Anderson, J.E., Genin, O., . . . Pines, M. (2008). Prevention of muscle fibrosis and improvement in muscle performance in the mdx mouse by halofuginone. Neuromuscular Disorders, 18(11), 857-868. doi:10.1016/j.nmd.2008.06.386

[22] Boldrin, L., Zammit, P.S., Morgan, J.E. (2015). Satellite cells from dystrophic muscle retain regenerative capacity. Stem Cell Research, 14(1), 20-29. doi:10.1016/j.scr.2014.10.007

[23] Mercado, M.L., Amenta, A.R., Hagiwara, H., Rafii, M.S., Lechner, B., Owens, R.T., . . . Fallon, J.R. (2006). Biglycan targets dystrobrevin, syntrophin and nNOS to the muscle cell membrane. The FASEB Journal, 20(10):1724-1726. doi:10.1096/fj.05-5124fje.

[24] Ito, M., Ehara, Y., Li, J., Inada, K., Ohno, K. (2017). Protein-Anchoring Therapy of Biglycan for Mdx Mouse Model of Duchenne Muscular Dystrophy. Human Gene Therapy, 28(5), 428-436. doi:10.1089/hum.2015.088

[25] Jaalouk, D.E., Lammerding, J. (2009). Mechanotransduction gone awry. Nature Reviews Molecular Cell Biology, 10(1), 63-73. doi:10.1038/nrm2597

[26] Rooney, J.E., Gurpur, P.B., Burkin, D.J. (2009). Laminin-111 protein therapy prevents muscle disease in the mdx mouse model for Duchenne muscular dystrophy. Proceedings of the National Academy of Sciences,106(19), 7991-7996. doi:10.1073/pnas.0811599106

[27] Naba, A., Clauser, K.R., Hoersch, S., Liu, H., Carr, S.A., Hynes, R.O. (2011). The Matrisome: In Silico Definition and In Vivo Characterization by Proteomics of Normal and Tumor Extracellular Matrices. Molecular & Cellular Proteomics, 11(4). doi:10.1074/mcp.m111.014647

[28] Naba, A., Clauser, K.R., Hynes, R.O. (2015). Enrichment of Extracellular Matrix Proteins from Tissues and Digestion into Peptides for Mass Spectrometry Analysis. Journal of Visualized Experiments, (101). doi:10.3791/53057

[29] Kaiser, P., Wohlschlegel, J. (2005). Identification of Ubiquitination Sites and Determination of Ubiquitin-Chain Architectures by Mass Spectrometry. Methods in Enzymology Ubiquitin and Protein Degradation, Part B, 399, 266-277. doi:10.1016/s0076-6879(05)99018-6

[30] Wang, Q., Barshop, W., Bian, M., Vashisht, A., He, R., Yu, X., . . . Lin, C. (2015). The Blue Light-Dependent Phosphorylation of the CCE Domain Determines the Photosensitivity of Arabidopsis CRY2. Molecular Plant, 8(4), 631-643. doi:10.1016/j.molp.2015.03.005

[31] Naba, A., Clauser, K.R., Ding, H., Whittaker, C.A., Carr, S.A., Hynes, R.O. (2016). The extracellular matrix: Tools and insights for the “omics” era. Matrix Biology, 49, 10-24. doi:10.1016/j.matbio.2015.06.003

[32] Holland, A., Murphy, S., Dowling, P., Ohlendieck, K. (2015). Pathoproteomic profiling of the skeletal muscle matrisome in dystrophinopathy associated myofibrosis. Proteomics, 16(2), 345-366. doi:10.1002/pmic.201500158

[33] Foidart, M., Foidart, J., Engel, W.K. (1981). Collagen Localization in Normal and Fibrotic Human Skeletal Muscle. Archives of Neurology, 38(3), 152-157. doi:10.1001/archneur.1981.00510030046006

[34] Duance, V.C., Stephens, H.R., Dunn, M., Bailey, A.J., Dubowitz, V. (1980). A role for collagen in the pathogenesis of muscular dystrophy? Nature, 284(5755), 470-472. doi:10.1038/284470a0

[35] Cynthia Martin, F., Hiller, M., Spitali, P., Oonk, S., Dalebout, H., Palmblad, M., . . .'t Hoen, P.A. (2014). Fibronectin is a serum biomarker for Duchenne muscular dystrophy. Proteomics Clinical Applications, 8:269–278. doi:10.1002/prca.201300072

[36] Schiavinato, A., Becker, A.A., Zanetti, M., Corallo, D., Milanetto, M., Bizzotto, D., . . . Bonaldo, P. (2012). EMILIN-3, Peculiar Member of Elastin Microfibril Interface-located Protein (EMILIN) Family, Has Distinct Expression Pattern, Forms Oligomeric Assemblies, and Serves as Transforming Growth Factor (TGF-) Antagonist. Journal of Biological Chemistry, 287(14), 11498-11515. doi:10.1074/jbc.m111.303578

[37] Burks, T.N., Cohn, R.D. (2011). Role of TGF-β signaling in inherited and acquired myopathies. Skeletal Muscle, 1(1), 19. doi:10.1186/2044-5040-1-19

[38] Allen, R.E., Boxhorn, L.K. (1987). Inhibition of skeletal muscle satellite cell differentiation by transforming growth factor-beta. Journal of Cellular Physiology, 133(3), 567-572. doi:10.1002/jcp.1041330319

[39] Mongiat, M., Fu, J., Oldershaw, R., Greenhalgh, R., Gown, A.M., Iozzo, R.V. (2003). Perlecan Protein Core Interacts with Extracellular Matrix Protein 1 (ECM1), a Glycoprotein Involved in Bone Formation and Angiogenesis. Journal of Biological Chemistry, 278(19), 17491-17499. doi:10.1074/jbc.m210529200

[40] Chan, I. (2004). The role of extracellular matrix protein 1 in human skin. Clinical and Experimental Dermatology, 29(1), 52-56. doi:10.1111/j.1365-2230.2004.01440.x

[41] Chan, I., El-Zurghany, A., Zendah, B., Benghazil, M., Oyama, N., Hamada, T., Mcgrath, J.A. (2003). Molecular basis of lipoid proteinosis in a Libyan family. Clinical and Experimental Dermatology, 28(5), 545-548. doi:10.1046/j.1365-2230.2003.01341.x

[42] Hamada, T. (2002). Lipoid proteinosis. Clinical and Experimental Dermatology, 27(8), 624-629. doi:10.1046/j.1365-2230.2002.01143.x

[43] Duan, C., Xu, Q. (2005). Roles of insulin-like growth factor (IGF) binding proteins in regulating IGF actions. General and Comparative Endocrinology,142(1-2), 44-52. doi:10.1016/j.ygcen.2004.12.022

[44] Henningsen, J., Rigbolt, K.T., Blagoev, B., Pedersen, B.K., Kratchmarova, I. (2010). Dynamics of the Skeletal Muscle Secretome during Myoblast Differentiation. Molecular & Cellular Proteomics, 9(11), 2482-2496. doi:10.1074/mcp.m110.002113

[45] Oh, Y., Nagalla, S.R., Yamanaka, Y., Kim, H.S., Wilson, E., Rosenfeld, R.G. (1996). Synthesis and characterization of insulin-like growth factor-binding protein (IGFBP)-7. Recombinant human mac25 protein specifically binds IGF-I and -II. The Journal of Biological Chemistry, 271(48): 30322-30325. doi:10.1074/jbc.271.48.30322

[46] Evdokimova, V., Tognon, C. E., Benatar, T., Yang, W., Krutikov, K., Pollak, M., . . . Seth, A. (2012). IGFBP7 Binds to the IGF-1 Receptor and Blocks Its Activation by Insulin-Like Growth Factors. Science Signaling, 5(255). doi:10.1126/scisignal.2003184

[47] Schiaffino, S., Mammucari, C. (2011). Regulation of skeletal muscle growth by the IGF1-Akt/PKB pathway: insights from genetic models. Skeletal Muscle, 1(1), 4. doi:10.1186/2044-5040-1-4

[48] Feitosa, N.M., Zhang, J., Carney, T.J., Metzger, M., Korzh, V., Bloch, W., Hammerschmidt, M. (2012). Hemicentin 2 and Fibulin 1 are required for epidermal–dermal junction formation and fin mesenchymal cell migration during zebrafish development. Developmental Biology, 369(2), 235-248. doi:10.1016/j.ydbio.2012.06.023

[49] Hopf, M., Gohring, W., Ries, A., Timpl, R., Hohenester, E. (2001). Crystal structure and mutational analysis of a perlecan-binding fragment of nidogen-1. Nature Structural Biology, 8(7):634–640. doi: 10.1038/89683

[50] Davies, J. A. (2001). Extracellular Matrix. ELS. doi:10.1038/npg.els.0001274

[51] Listrat, A., Lebret, B., Louveau, I., Astruc, T., Bonnet, M., Lefaucheur, L., . . . Bugeon, J. (2016). How Muscle Structure and Composition Influence Meat and Flesh Quality. The Scientific World Journal, 2016, 1-14. doi:10.1155/2016/3182746

[52] Gillies, A.R., Lieber, R.L. (2011). Structure and function of the skeletal muscle extracellular matrix. Muscle & Nerve, 44(3), 318-331. doi:10.1002/mus.22094

[53] Lawrie, R. (1989). Connective tissue in meat and meat products. Meat Science, 26(4), 325-326. doi:10.1016/0309-1740(89)90016-8

[54] Bernardo, B.C., Belluoccio, D., Rowley, L., Little, C.B., Hansen, U., Bateman, J.F. (2011). Cartilage Intermediate Layer Protein 2 (CILP-2) Is Expressed in Articular and Meniscal Cartilage and Down-regulated in Experimental Osteoarthritis. Journal of Biological Chemistry, 286(43), 37758-37767. doi:10.1074/jbc.m111.248039

[55] Johnson, K., Farley, D., Hu, S., Terkeltaub, R. (2003). One of two chondrocyte-expressed isoforms of cartilage intermediate-layer protein functions as an insulin-like growth factor 1 antagonist. Arthritis & Rheumatism, 48(5), 1302-1314. doi:10.1002/art.10927

[56] Shindo, K., Asakura, M., Min, K., Ito, S., Fu, H.Y., Yamazaki, S., . . . Kitakaze, M. (2017). Cartilage Intermediate Layer Protein 1 Suppresses TGF-β Signaling in Cardiac Fibroblasts. International Journal of Gerontology. doi:10.1016/j.ijge.2017.01.002